CORECOOL. Model description of the programme

Forskningscenter Risø, Roskilde; Abel-Larsen, H.

Publication date:
1978

Document Version
Publisher's PDF, also known as Version of record

Risø-M-2138

Department of Reactor Technology
Risø National Laboratory
DK-4000 Roskilde
Denmark

Risø-M-2138
(August 1975)
November 1978

CORECOOL

Model Description of the Programme

by

Jens G. Munthe Andersen
H. Abel-Larsen

Risø

Risø - M - 2138

Risø - M - 2138

Title and author(s)

CORECOOL
Model Description of the Programme

by

Jens G. Munthe Andersen
H. Abel-Larsen

Date November 1978

Department or group

Department of Reactor Technology

Group's own registration number(s)

pages + tables + illustrations

Abstract

CORECOOL, Convection and Radiation Emergency Cooling, is a model for the two-phase flow and heat transfer in a fuel element during the core heat-up phase following a loss of coolant accident. The model for the two-phase flow is based on a solution of the conservation equations with a separate description of the two phases and thermodynamic non-equilibrium. The flow-regimes considered are drop flow and film flow. The heat transfer consists of convection, sputtering and radiation heat transfer.

The documentation of CORECOOL consists of four parts:

Part I: Model Description
Part II: Programme Description (COMMERCIAL)
Part III: Users Guide (COMMERCIAL)
Part IV: Verification.(COMMERCIAL)

CORECOOL is a joint project between Risø National Laboratory and General Electric Company, San José, USA.

Copies to

Biblioteket 100
Reaktorteknik 25

Available on request from Risø Library, Risø National Laboratory (Risø Bibliotek, Forsøgsanlæg Risø), DK-4000 Roskilde, Denmark
Telephone: (03) 37 12 12 ext.2262, telex: 43116

f. 25-204

ISBN 87-550-0565-9
ISSN 0418-6435

CONTENTS

1. INTRODUCTION

CORECOOL, Convection and Radiation Emergency Cooling, is a model for evaluation of core heat-up transients for a fuel element and for evaluation of the performance of the spray system. CORECOOL applies to the phase of a loss of coolant accident, LOCA, after the termination of the blow-down, i.e. the core is uncovered and there is pressure equilibrium between the vessel and the containment. The model applies as well to nuclear reactor fuel element as to electrical heated test elements used for simulation of a LOCA.

CORECOOL consists of two basic models, a fuel rod model and a model for the two-phase flow in the system. The fuel rod model is a heat conduction model, which is also applied to the channel. The two-phase flow model is based on solution of the conservation equations for mass, momentum and energy, and the equation of state. The two phases are treated separately, and physical models and correlations are developed for the interchange of mass, momentum and energy. Thermodynamic equilibrium is not assumed, and the steam is allowed to be superheated and the water subcooled. The coupling between the fuel rod model and the two-phase flow model is taken into account through a number of physical models and correlations for the heat transfer, which includes conduction, convection and thermal radiation.

The approach of CORECOOL is to develop a model which is more based on a sophisticated analysis of the different physical and chemical phenomena, and not on gross system dependent empirical correlations. This approach, besides giving a better understanding, makes the model system independent.

The independence of the system makes parametic studies and sensitivity analysis possible and reduces the need for expensive experiments.

CORECOOL is a further development of the model REMI/HEATCOOL[1].

2. BASIC MODELS

CORECOOL models a fuel element and a corresponding part of the primary system, which is scaled down to one fuel element, cf. fig. 2.1. The model for the fuel element include the fuel rods and the channel whereas the rest of the primary system is represented as a set of connected flowpaths and volumes.

The physical model contains an energy equation for the fuel rods and the channel, and the conservation equations for the two-phase flow in the system. The conservation equations for the two-phase flow are written as separate equations for the two phases and allows thermodynamic non equilibrium and consideration of counter current flow. A number of constitutive equations such as heat transfer correlations including conduction, convection and radiation heat transfer accounts for the coupling between the energy equation for the fuel rods and the conservation equations for the two-phase flow, cf. fig. 2.2.

2.1. The Geometrical Model

The model in CORECOOL contains a representation of the lower plenum, one fuel element, the upper plenum, risers and separators, the steamdome and the downcomer including the pumps. The break may be anywhere in the downcomer region from the lower plenum to the steam dome. The different regions are subdivided into an arbitrary number of nodes, and the regions are connected in form of a loop, cf. fig. 2.3.

Each rod represented individually in the fuel element and the channel is represented as a square box, cf. fig. 2.4. The fuel rods may, however, due to symmetry be combined to a number of rod groups for which identical behaviour are assumed. The upper and lower tie plate and the spacers in the fuel element are only represented through their loss coefficients.

The spray nozzel is placed in the top of the upper plenum, just below the risers.

2.2. Two-Phase Flow Model, the Conservation Equations

The treatment of the two-phase flow in CORECOOL is based on the solution of the one-dimensional equations for conservation of

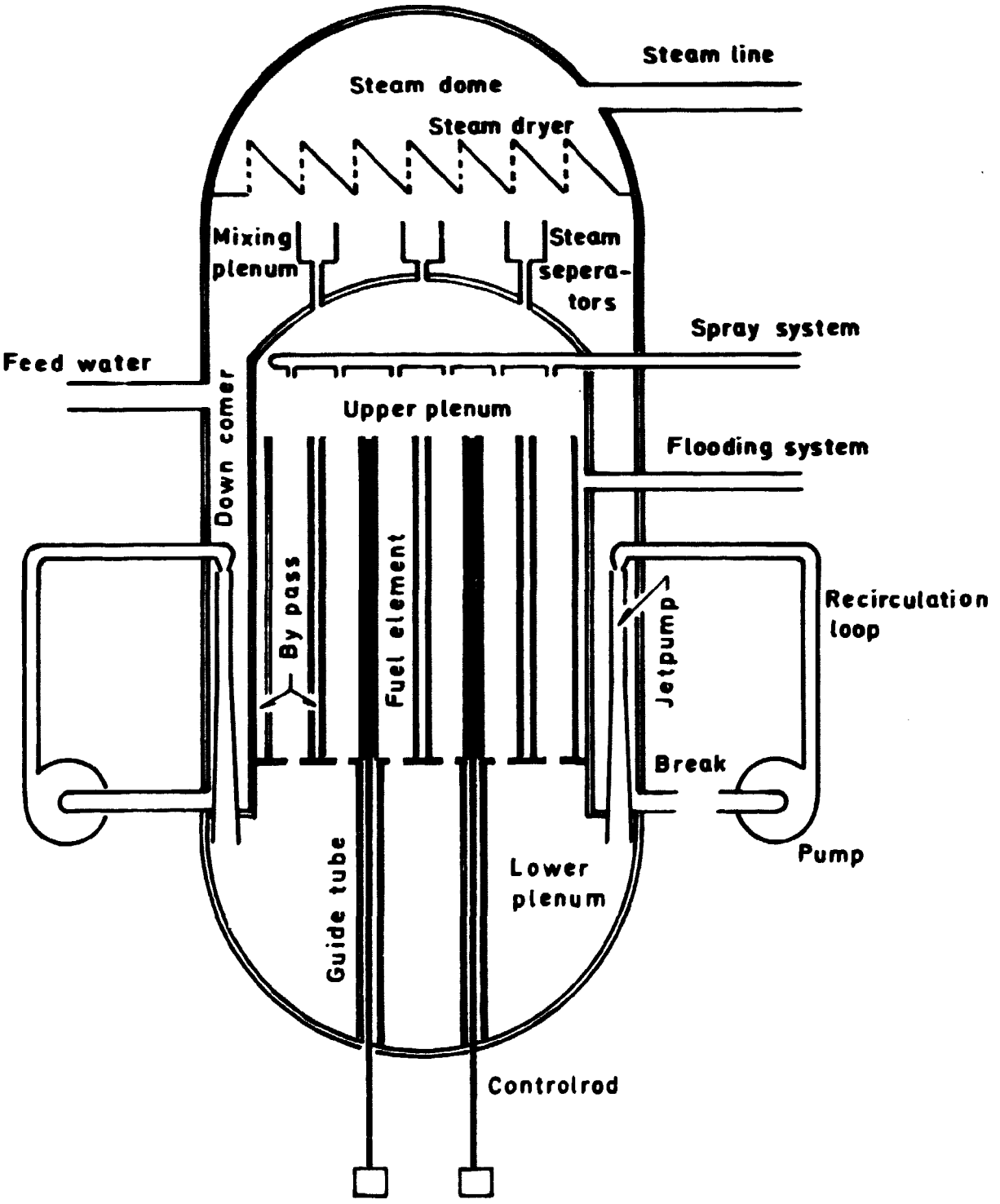

Fig. 2.1. Reactor Vessel and Primary System

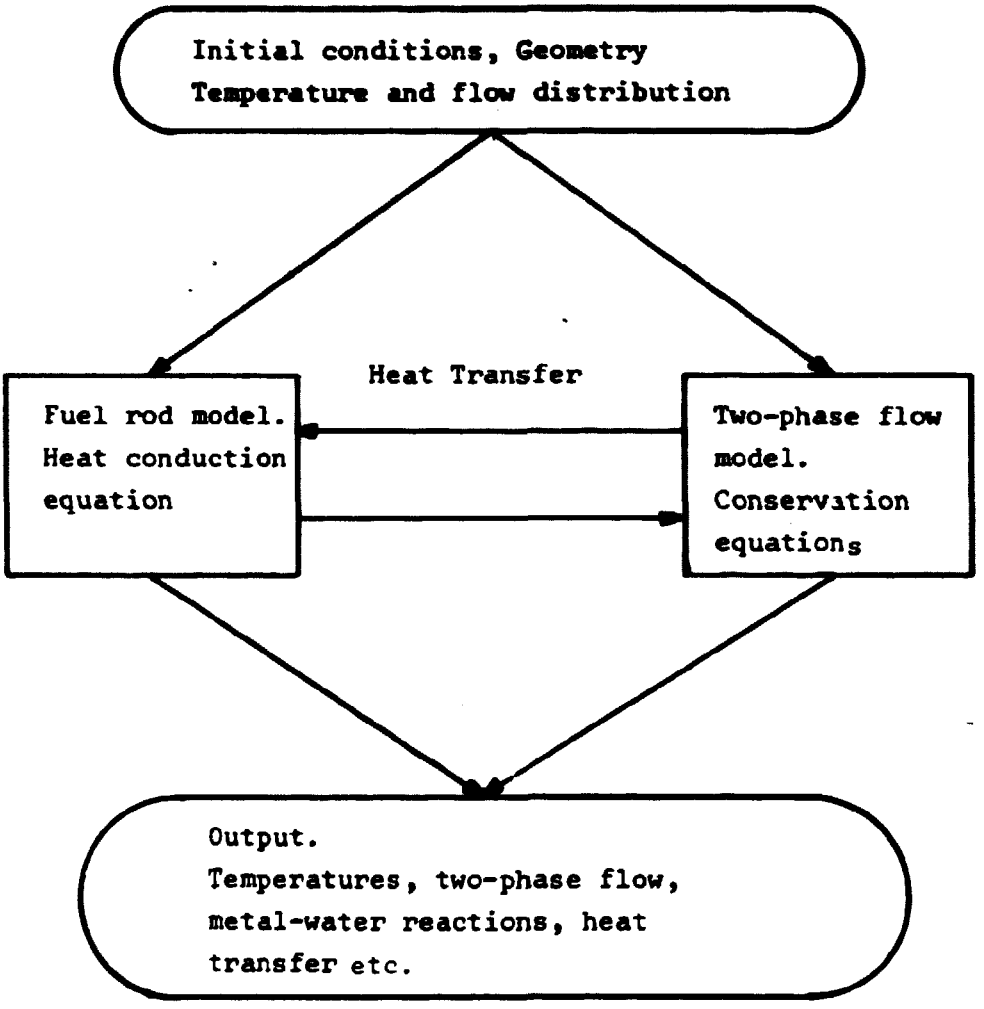

Fig. 2.2. CORECOOL Physical Model.

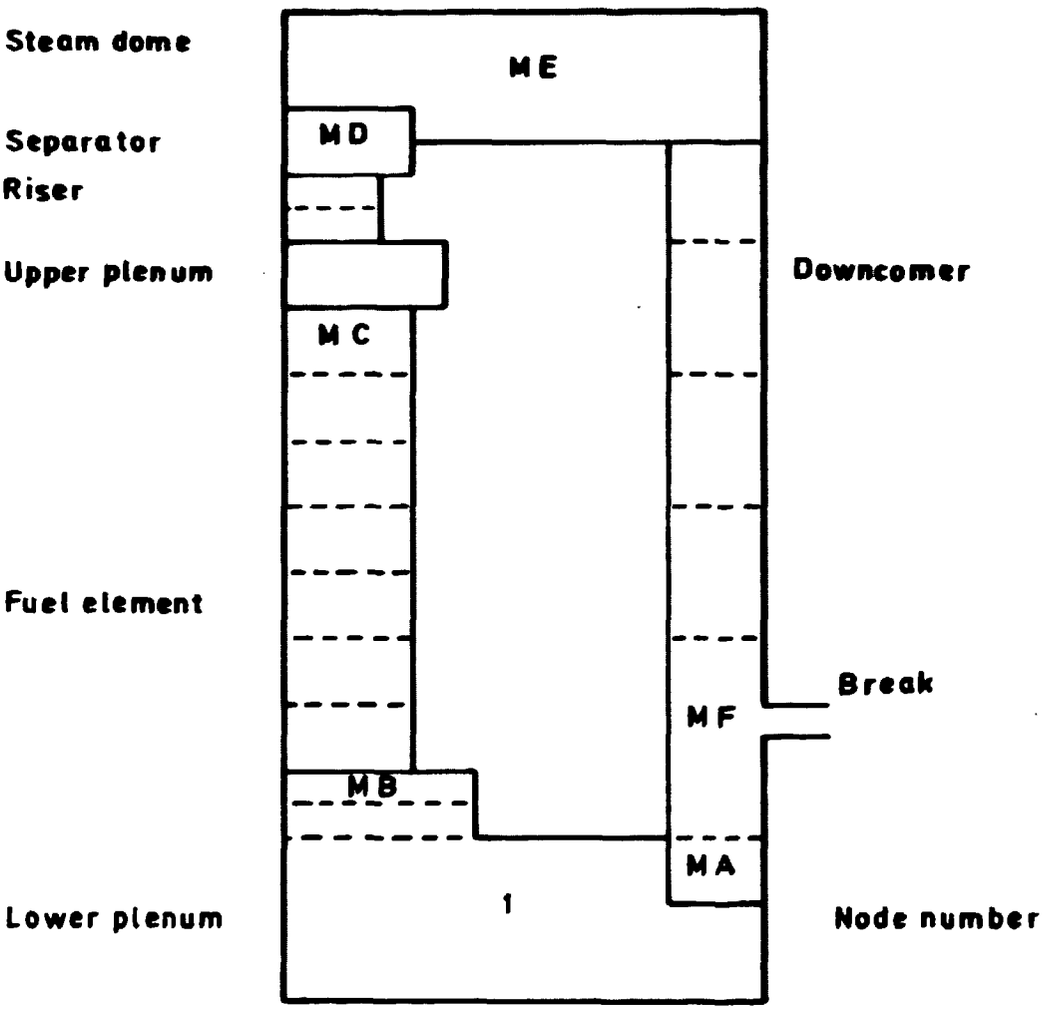

Fig.2.3. Nodalization of CORECOOL-Model.

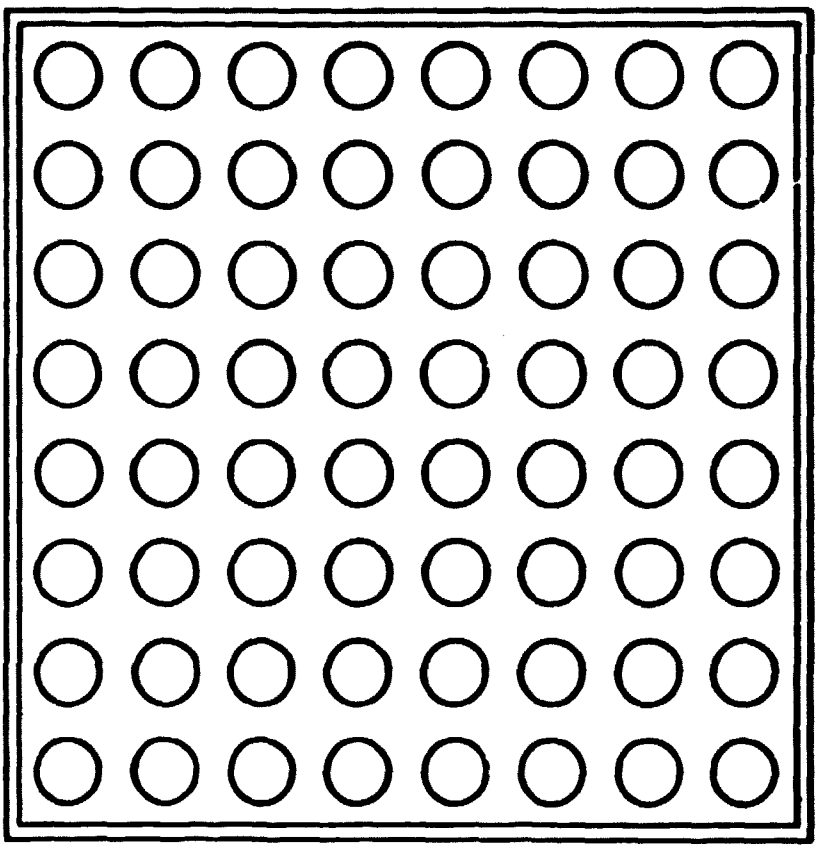

Fig. 2.4. Cross Section of CORECOOL Fuel Element

mass, momentum and energy, and the equation of state. The steam and water phases are treated separately in order to allow counter current flow, and the interactions between the phases are considered through constitutive equations for the interfacial mass, momentum and energy transfer.

Thermodynamic equilibrium is not assumed, i.e. the steam is allowed to be superheated and the water to be subcooled.

However, due to a priory knowledge about the flowregime some simplificating assumptions can be made. The characteristics of the two-phase flow during the core heat-up transient with spray cooling are

1. The flow regimes are drop-flow and film-flow, and the void fraction is close to unity.
2. The flow-rates are small and the Reynolds numbers are in the order of 1000 - 3000.
3. The transient is slow and fast variations in pressure and velocities, i.e. effects related to the velocity of sound, are negligible.

Based on these characteristics of the two-phase flow the following assumptions can be made.

a. In the momentum equation for the steam the time derivative is negligible.

$$\frac{\partial}{\partial t}(\rho_g u_g) \approx 0.0$$

b. In the energy equations the time derivative of the pressure, and the kinetic and potential energy are negligible.

$$\frac{\partial p}{\partial t} \approx 0.0$$

$$\tfrac{1}{2}\rho u^2 + \rho g z \approx 0.0$$

2.2.1. The Continuity Equations

The one-dimensional conservation equations for mass for the steam and water[1,2,3] are given by

$$\frac{\partial}{\partial t}(\alpha A \rho_g) = -\frac{\partial}{\partial z} W_g + A(\phi_{lg} + \dot{m}_g) \qquad (2.1)$$

$$\frac{\partial}{\partial t}((1-\alpha) A \rho_l) = -\frac{\partial}{\partial z} W_l + A(-\phi_{lg} + \dot{m}_l) \qquad (2.2)$$

where ϕ is evaporation/condensation, and $\dot{m}_g$ and $\dot{m}_l$ are source terms, e.g. the spray system. Integration of equations 2.1 and 2.2 over a control volume yields, cf. fig. 2.5.

$$\frac{\partial}{\partial t}(\alpha V\rho_g) = -(W_g)_{z_i}^{z_o} + V(\phi_{lg} + \dot{m}_g) \tag{2.3}$$

$$\frac{\partial}{\partial t}((1-\alpha)V\rho_l) = -(W_l)_{z_i}^{z_o} + V(-\phi_{lg} + \dot{m}_l) \tag{2.4}$$

where

$$V = A\Delta z \tag{2.5}$$

For the droplets, besides the mass, also the number density has to be conserved. The conservation of droplets, neglecting combination and break up of the droplets, is given by

$$\frac{\partial}{\partial t}(A\, n_d) = -\frac{\partial}{\partial z}(\Omega_d\, n_d) + A\,\dot{n}_d \tag{2.6}$$

Note that evaporation/condensation does not change the concentration of droplets, only the mass and diameter, but a source term is still needed. Integration of equation 2.6 over a control volume gives

$$\frac{\partial}{\partial t}(V\, n_d) = -(\Omega_d\, n_d)_{z_i}^{z_o} + V\,\dot{n}_d \tag{2.7}$$

The diameter of the droplets is given by

$$(1-\alpha) = \frac{\pi}{6} d_d^3\, n_d \tag{2.8}$$

2.2.2. The Momentum Equations

The one-dimensional conservation equations for momentum[1,2,3] for the steam and water are given by

$$\frac{\partial}{\partial t}(\alpha A \rho_g u_g) = -\frac{\partial}{\partial z}(c_g W_g u_g) - \alpha A \frac{\partial P}{\partial z} - A f_g - A\alpha\rho_g g\cos\theta + A\phi_{lg} u^{\wedge} + A b_{lg} + A\dot{B}_g \tag{2.9}$$

$$\frac{\partial}{\partial t}((1-\alpha)A\rho_l u_l) = -\frac{\partial}{\partial z}(c_l W_l u_l) - (1-\alpha)A\frac{\partial P}{\partial z} - A f_l - A(1-\alpha)\rho_l g\cos\theta - A\phi_{lg} u^{\wedge} - Ab_{lg} + A\dot{B}_l \tag{2.10}$$

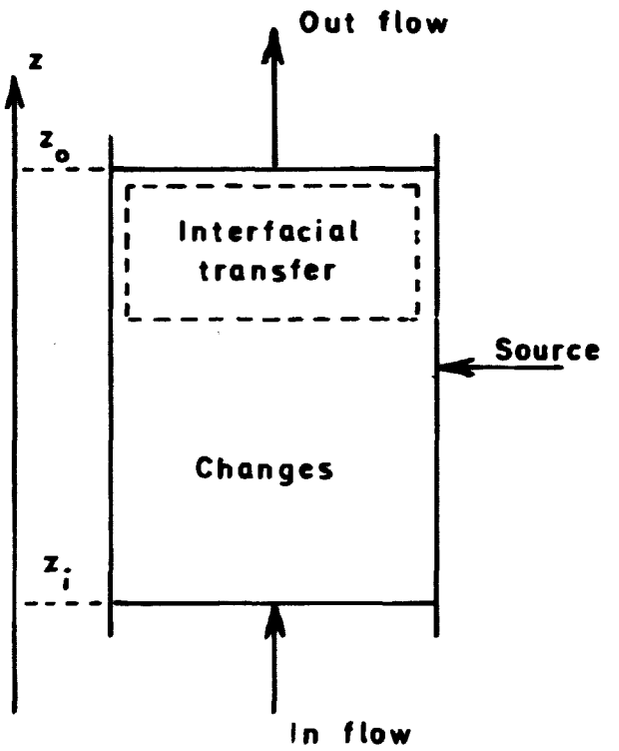

Fig. 2.5. Control Volume for One-Dimensional Two-Phase Flow

$$\text{where } u` = \begin{cases} u_l \text{ for evaporation, } \phi_{lg} > 0 \\ u_g \text{ for condensation, } \phi_{lg} \leq 0 \end{cases} \tag{2.11}$$

b_{lg} is the interfacial shear, and $\dot{B}_g$ and $\dot{B}_l$ are source terms. The first term on the right hand side of equation 2.9 can be written as

$$\frac{\partial}{\partial z}(c_g W_g u_g) = \alpha A \frac{\partial}{\partial z}(c_g \rho_g u_g^2) + c_g \rho_g u_g^2 \{\alpha \frac{\partial A}{\partial z} + A \frac{\partial \alpha}{\partial z}\} \tag{2.12}$$

Using 1 and 3 in section 2.2. we can make the approximation

$$\frac{\partial \alpha}{\partial t} \simeq 0.0 \text{ and } \frac{\partial \dot{\alpha}}{\partial z} \simeq 0.0 \text{ in equation 2.9.} \tag{2.13}$$

As the model in CORECOOL consists of constant area ducts $\frac{\partial A}{\partial z} = 0$, and irreversible pressure drops due to area changes can be included in f_g through a loss coefficient, (2.9) can be rewritten to

$$\frac{\partial}{\partial t}(\rho_g u_g) = -\frac{\partial}{\partial z}(c_g \rho_g u_g^2) - \frac{\partial P}{\partial z} - \frac{f_g}{\alpha} - \rho_g g \cos\theta + \frac{\phi_{lg} u` + b_{lg} + \dot{B}_g}{\alpha} \tag{2.14}$$

Defining

$$I_g = \oint \rho_g u_g \, dz \tag{2.15}$$

we get

$$\frac{d}{dt} I_g = \oint \left\{ -\rho_g g \cos\theta + \frac{-f_g + \phi_{lg} u` + b_{lg} + \dot{B}_g}{\alpha} \right\} dz \tag{2.16}$$

Integrating equation 2.10 over a control volume yields

$$\frac{\partial}{\partial t}((1-\alpha) V \rho_l u_l) = -\left[c_l W_l u_l \right]_{z_i}^{z_o} + V \left\{ -(1-\alpha)\frac{\partial P}{\partial z} - f_l - (1-\alpha)\rho_l g \cos\theta - \phi_{lg}` u` - b_{lg} + \dot{B}_l \right\} \tag{2.17}$$

In CORECOOL c_l and c_g are set equal to 1.

2.2.3. The Energy Equations

The one-dimensional conservation equations for energy[1,2,3] for the steam and the water are given by

$$\frac{\partial}{\partial t}(\alpha A(\rho_g h_g - P)) = -\frac{\partial}{\partial z}(W_g h_g) + S_g q_g'' - A q_{gl}''' + A \phi_{lg} h_{sg} + A Q_g''' - A P \frac{\partial \alpha}{\partial t} \quad (2.18)$$

$$\frac{\partial}{\partial t}((1-\alpha)A(\rho_l h_l - P)) = -\frac{\partial}{\partial z}(W_l h_l) + S_l q_l'' + A q_{gl}''' - A \phi_{lg} h_{sg} + A Q_l''' + A P \frac{\partial \alpha}{\partial t} \quad (2.19)$$

q_{gl}''' is interfacial heat transfer from the steam to the steam-water interface, and Q_g''' and Q_l''' are sources. Defining q_{lg}''' as the interfacial heat transfer from the steam-water interface to the water, the conservation of mass and energy gives, cf. fig. 2.6

$$\phi_{lg} = \frac{q_{gl}''' - q_{lg}'''}{h_{lg}} \quad (2.20)$$

Using b in section 2.2, $\frac{\partial P}{\partial t} \approx 0$, and integrating over a control volume gives

$$\frac{\partial}{\partial t}(\alpha V \rho_g h_g) = -\left(W_g h_g\right)_{z_i}^{z_o} + S_g \Delta z\, q_g'' - V q_{gl}''' + V \phi_{lg} h_{sg} + V Q_g''' \quad (2.21)$$

$$\frac{\partial}{\partial t}((1-\alpha)V \rho_l h_l) = -\left(W_l h_l\right)_{z_i}^{z_o} + S_l \Delta z\, q_l'' + V q_{gl}''' - V \phi_{lg} h_{sg} + V Q_l''' \quad (2.22)$$

2.2.4. Integration of the Conservation Equations

Except for the integration of I_g (cf. eq. 2.15 and 2.16), where the explicit Euler method is used, the integration technique is the modified Euler method with linearization of the non-linear terms.

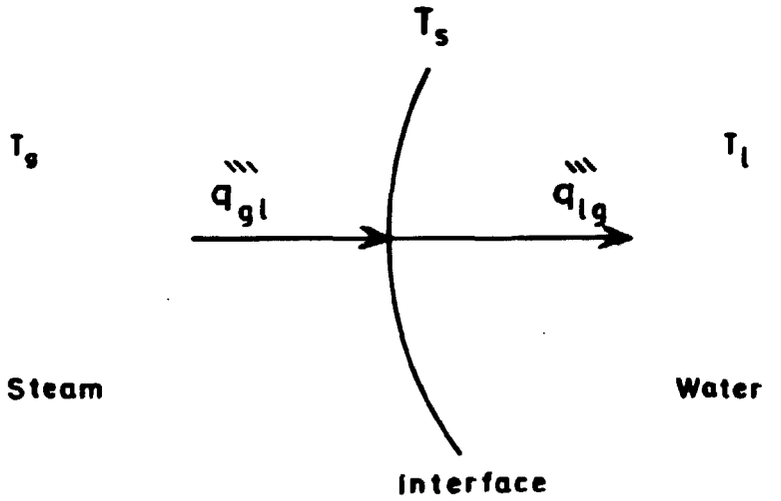

$$\varphi_{lg} = \frac{q'''_{gl} - q'''_{lg}}{h_{lg}}$$

Fig. 2.6. Heat and Mass Transfer at Steam-Water Interface

2.2.4.1. Integration of the Conservation Equations for the Steam. Multiplying equation 2.3 with h_g and subtracting it from equation 2.21 we get

$$\alpha V \rho_g \frac{\partial h_g}{\partial t} = -\left(W_g h_g\right)\Big|_{z_i}^{z_o} + S_g \Delta z\, q_g'' - V q_{gl}''' + V \phi_{lg} h_{sg} + V Q_g''' + h_g \left(W_g\right)\Big|_{z_i}^{z_o} - V(\phi_{lg} + \dot{m}_g) h_g \qquad (2.23)$$

Equation (2.23) is integrated using the modified Euler method with liniarization. Using 3 in section 2.2, $\frac{\partial P}{\partial t} \approx 0$. we get

$$\rho_g = \rho_g(h_g, P) \qquad (2.24)$$

$$T_g = T_g(h_g, P) \qquad (2.25)$$

$$\frac{\partial \rho_g}{\partial t} = \frac{\partial \rho_g}{\partial h_g} \frac{\partial h_g}{\partial t} \qquad (2.26)$$

Equation 2.16 is integrated directly using the Euler method.

Let $W_{g,ci}$ be the steam flow at the core inlet, then combining equations 2.1 and 2.15 we get

$$W_g = W_{g,ci} + \int_{z_{ci}}^{z} \left\{ A(\phi_{lg} + \dot{m}_g) - \alpha A \frac{\partial \rho_g}{\partial t} - \rho_g A \frac{\partial \alpha}{\partial t} \right\} ds \qquad (2.27)$$

$$W_{g,ci} = \frac{I_g - \oint \frac{1}{\alpha A} \left\{ \int_{z_{ci}}^{z} (A(\phi_{lg} + \dot{m}_g) - \alpha A \frac{\partial \rho_g}{\partial t} - \rho_g A \frac{\partial \alpha}{\partial t}) ds \right\} dz}{\oint \frac{1}{\alpha A} dz} \qquad (2.28)$$

$W_{g,ci}$ is found from equation 2.28 and the steam flow rates from equation 2.27. The pressure distribution is then found from (2.9) neglecting the time derivatives.

2.2.4.2. Integration of the Conservation Equations for the Water. The conservation equations for the drop flow are integrated directly using the modified Euler method with linearizations for ρ_d, n_d, u_d and h_d. The temperature of the droplets is given by

$$T_d = T_d(h_d) \tag{2.29}$$

neglecting the dependence of pressure in the equation of state.

For the film flow the quasi steady state solution to the momentum equation

$$W_f = -S \frac{\rho_f(\rho_f - \rho_g)g}{3\mu} s_f^3 \tag{2.30}$$

is used, and the continuity and energy equations are integrated using the modified Euler method with linearization.

2.3. Fuel Rod Model, the Fourier Equation

In the fuel rods axial conduction is neglected, and the one-dimensional heat conduction equation becomes[1)]

$$\rho\, c \frac{\partial}{\partial t}(T) = \frac{1}{r} \frac{\partial}{\partial r} (r\, k \frac{\partial T}{\partial r}) + q''' \tag{2.31}$$

Here ρ and c are functions of the temperature.

Making an energy balance for a control volume as shown in fig. 2.7 gives

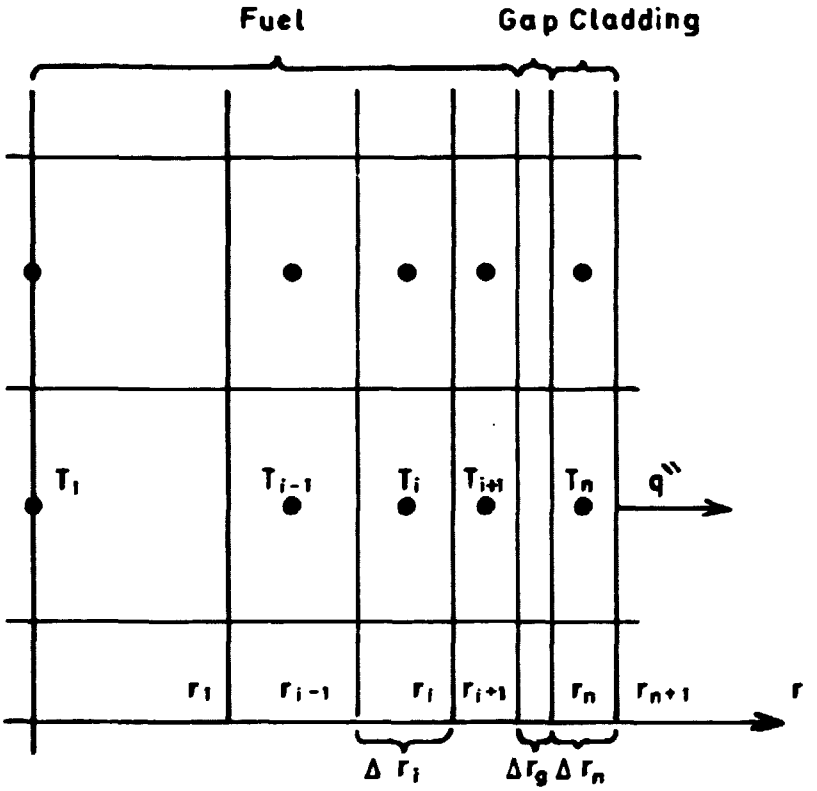

Fig.2.7.Finite Difference Mesh for Fuel Rod

$$\pi(r_i^2-r_{i-1}^2)\Delta z\ \rho_i c_i \frac{\partial T_i}{\partial t} = \frac{4\ k_{i-1}\ k_i\ \pi\ r_{i-1}\Delta z}{\Delta r_i\ k_{i-1}+\Delta r_{i-1}\ k_i}(T_{i-1}-T_i)$$

$$- \frac{4\ k_i\ k_{i+1}\ \pi\ r_i\ \Delta z}{\Delta r_{i+1}\ k_i+\Delta r_i\ k_{i+1}}(T_i-T_{i+1})$$

$$+ \pi(r_i^2 - r_{i-1}^2)\Delta z\ q''' \qquad (2.32)$$

If a node is next to the gas gap, the gas gap heat transfer coefficient has to be considered in the conduction heat transfer, and similary for the cladding the surface heat flux has to be considered. For the outer fuel node, node n-1, we get

$$\pi(r_{n-1}^2-r_{n-2}^2)\Delta z\ \rho_{n-1}\ c_{n-1} \frac{\partial T_{n-1}}{\partial t} = \frac{4\ k_{n-2}\ k_{n-1}\ \pi\ r_{n-2}\ \Delta z}{\Delta r_{n-1}\ k_{n-2}+\Delta r_{n-2}\ k_{n-1}}(T_{n-2}-T_{n-1})$$

$$- \frac{2\pi(r_{n-1}+r_n)\Delta z}{\frac{\Delta r_{n-1}}{k_{n-1}} + \frac{2}{h_{gab}} + \frac{\Delta r_n}{k_n}}(T_{n-1}-T_n)$$

$$+ \pi(r_{n-1}^2-r_{n-2}^2)\Delta z\ q''' \qquad (2.33)$$

and for the cladding node, node n,

$$\pi(r_{n+1}^2-r_n^2)\Delta z\ \rho_n\ c_n \frac{\partial T_n}{\partial t} = \frac{2\pi(r_{n-1}+r_n)\Delta z}{\frac{\Delta r_{n-1}}{k_{n-1}} + \frac{2}{h_{gab}} + \frac{\Delta r_n}{k_n}}(T_{n-1}-T_n)$$

$$- 2\pi\ r_{n+1}\ \Delta z\ q'' + \pi(r_{n+1}^2-r_n^2)\Delta z\ q''' \qquad (2.34)$$

The equations 2.32 - 2.34 are integrated using the implicit Cranck-Nicholson scheme.

For the channel only one node is used and the analysis is a lumped analysis. A direct explicit integration technique is used.

3. CORRELATIONS AND PHYSICAL MODELS

A variety of correlations and physical models are used in CORECOOL, not only in the coupling between the heat conduction model and the two-phase flow model, but also in the models themselves. In the fuel-rod model, correlations and physical models exist e.g. for the energy generation due to decay heat and the metal-water reaction, and for the heat transfer across the gas gap. For the two-phase flow a number of correlations exist for the interfacial mass, momentum and energy transfer.

The correlations and physical models can be arranged in two main groups, models related to the momentum transfer and models related to the energy generation and transfer. The momentum transfer includes such models as interfacial shear and wall shear, models for the formation of droplets from the spray nozzel, and counter current flow limitation. The heat transfer consists of conduction, convection and radiation heat transfer.

3.1. Momentum Transfer

Momentum transfer exists in a number of different ways in CORECOOL. It exsists as shear between the wall and the two-phase flow, and as interfacial shear between the steam and water. Irreversible pressure losses from area changes or flow restrictions are also treated as shear, and are represented through a loss coefficient.

The shear is important not only in the determination of the pressure drops and the velocity distribution of the two phases, but also for the dropletsize. It is a balance between the shear forces and the surface tension which determines the break up of the water from the nozzels into droplets and the size of these droplets. The shear is also an important parameter for the counter current flow limitation.

3.1.1. Wall Shear

The flow regimes under consideration in CORECOOL are drop flow and filmflow. The shear between a film and the wall is

mainly viscous shear and will be treated in section 3.1.2.

For the dropflow the void fraction will generally be very high, typically between 0.95 and 1.0, and as the interfacial shear between the droplets and the steam is calculated separately, cf. section 3.1.4, the wall shear is calculated as single phase friction for the steam.

The friction is calculated as, cf. equation 2.9,

$$f_g = \tfrac{1}{2}\,\rho_g\,u_g|u_g|\,4\,\frac{C_F}{D_h} \tag{3.1}$$

where the friction factor is given by [2)]

$$C_F = \begin{cases} \dfrac{16}{Re_g} & \text{for laminar flow} \qquad (3.2) \\ 0.0792 \cdot Re_g^{-0.25} & \text{for turbulent flow} \qquad (3.3) \end{cases}$$

$$Re_g = \frac{\rho_g\,D_h|u_g|}{\mu_g} \tag{3.4}$$

The transition between the two correlations is for numerical reasons made at the inter section, $Re_g = 1185.4$, and not at the true transition which takes place at a Reynolds number just above 2000 (cf. fig. 3.1).

3.1.2. The Falling Film

The other important flow regime in CORECOOL is the film flow regime. In this case the rods or the channel are covered with a falling film, and the core of the flow is either dropflow or single phase steam flow.

The film flow is mainly determined as a balance between the gravity and the viscous shear at the wall. Shear does exist between the film and the core of the flow, but is negligible for the film flow. A quasi steady state approach is used in CORECOOL given by [2)]

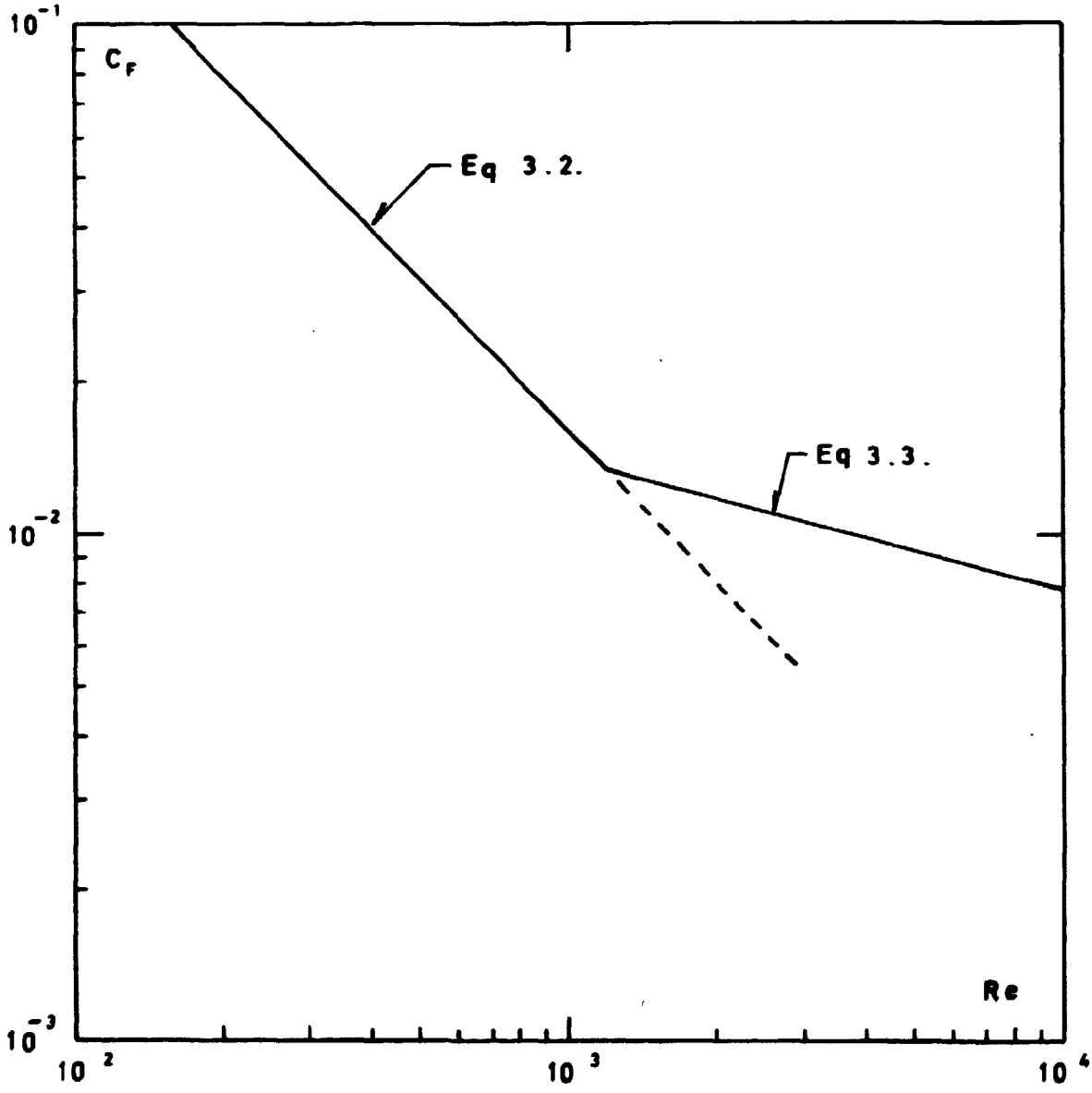

Fig. 3.1. Single phase friction factor.

$$G_f = - \frac{\rho_f(\rho_f-\rho_g)g}{3\mu_f} d_f^3 \qquad (3.5)$$

The flow rates existing during ECCS transients are such that the Reynolds number

$$Re_f = \frac{G_f}{\mu_f} \qquad (3.6)$$

is generally less than 500, where the flow is laminar and (3.5) is valid.

3.1.3. Loss Coefficients

Irreversible pressure losses arises from area changes or flow restrictions such as spacers, the upper tie plate etc. These pressure losses are calculated as a product between the dynamic head of the steam, as the steam is the continuous phase, and a loss coefficient

$$\Delta P = \tfrac{1}{2} \rho_g u_g^2 C_L \qquad (3.7)$$

Besides simple flow restrictions also the pressure drops through the risers, steam separators, and the pump are calculated through a loss coefficient.

3.1.4. Interfacial Shear

Interfacial shear exists between the steam flow and the film flow, and between the droplets and the steam.

For the falling film the interfacial shear, as stated in section 3.1.2, is negligible, and as the film velocity generally is much smaller than the steam velocity, the film velocity may be neglected in the calculation of the shear on the steam. The shear on the steam is thus calculated in the same way as the wall shear, cf. section 3.1.1.

The interfacial shear between the steam and the droplets may be calculated through the use of a drag-coefficient

$$b_{lg} = -n_d \tfrac{1}{8} \rho_g (u_g - u_d)|u_g - u_d| \tfrac{\pi}{4} d_d^2 C_D \qquad (3.8)$$

For a single spherical droplet in an infinite medium the drag coefficient is given by[1,3)]

$$C_{D_s} = \begin{cases} \frac{24}{Re_d} & \text{for } Re_d < 0.71 \\ 0.4 + 25.4\, Re_d^{-0.25} & \text{for } Re_d \geq 0.71 \end{cases} \qquad (3.9)$$

where

$$Re_d = \frac{\rho_g d_d |u_g - u_d|}{\mu_g} \qquad (3.10)$$

Two phenomena will affect this result. For large droplets, the droplets will be distorted from the spherical shape, and the equilibrium velocity of the droplet tend to be independent of the size[2)]. A typical droplet size in a fuel bundle is about 2 mm, as most of the droplets originates from a sputtering front, and the Weber number will be around 2, which is much smaller than the critical Weber number of 13. Accordingly the droplets will be nearly spherical, and equation 3.9 is a good correlation for the drag. The other phenomenon which affects the drag is the presence of other droplets. The larger the droplet concentration is, the larger the drag will be. Wallis[2)] gives the following relation for the influence of neighbour droplets

$$C_D = \frac{C_{D_s}}{\alpha^2} \qquad (3.11)$$

3.1.5. The Spray Nozzel

A general model for the spray nozzel is difficult to make. The way the liquid leaves the nozzel, how it breaks up into droplets and how these droplets may break up into smaller droplets, will depend very much on the construction of the nozzel. However, a simple semiempirical model is made. The model contains two characteristic parameters, which properly chosen describes the nozzel very well over wide range of flow rates.

For most of the nozzels used for ECC purposes the water will leave the nozzel either in form of a single jet or in form of a cone. This cone is modelled as a set, N_j, of liquid jets leaving

in all directions inside the cone, cf. fig. 3.[illegible]. Each of these jets will then due to the Helmholz instability[4] break up into droplets, and if the Weber number of these droplets is larger than 13 they will be unstable and break up into smaller droplets as long as the Weber number is larger than 13. A detailed derivation is given in appendix A.

A small sinosoudial perturbation on one of the jets leaving the nozzel will neglecting the viscosity, grow with a growth rate given by

$$\omega^2 = \frac{\sigma}{2\rho_\ell r_j^3}(\lambda r_j)^2\left\{1-(\lambda r_j)^2+\lambda r_j\frac{We_j}{2}\right\} \tag{3.12}$$

where

$$We_j = \frac{\rho_g d_j(u_g-v_j)^2}{\sigma} \tag{3.13}$$

Differentiating (3.12) it is easily found that the maximum growth rate occurs for

$$\lambda r_j = \frac{3}{16}We_j + \sqrt{(\frac{3}{16}We_j)^2+\frac{1}{2}} \tag{3.14}$$

which gives the diameter of the produced droplets

$$d_d = d_j\left\{\frac{3\pi}{\frac{3}{8}We_j+\sqrt{(\frac{3}{8}We_j)^2+2}}\right\}^{\frac{1}{3}}. \tag{3.15}$$

From equation 3.12 and 3.14 the length of the jets can be found to

$$L_j = r_j\ln(\frac{r_j}{\Delta r_j})\sqrt{\frac{\rho_\ell}{\rho_g}}\frac{\sqrt{We_j}}{\left\{\frac{3}{16}We_j+\sqrt{(\frac{3}{16}We_j)^2+\frac{1}{2}}\right\}\left\{\frac{1}{2}+\frac{3}{128}We_j^2+\frac{We_j}{8}\sqrt{(\frac{3}{16}We_j)^2+2}\right\}^{\frac{1}{2}}}$$

where Δr_j is the initial perturbation. Comparisons with experiments gives[5]

$$\ln(\frac{r_j}{\Delta r}) \approx 15.7 \tag{3.16}$$

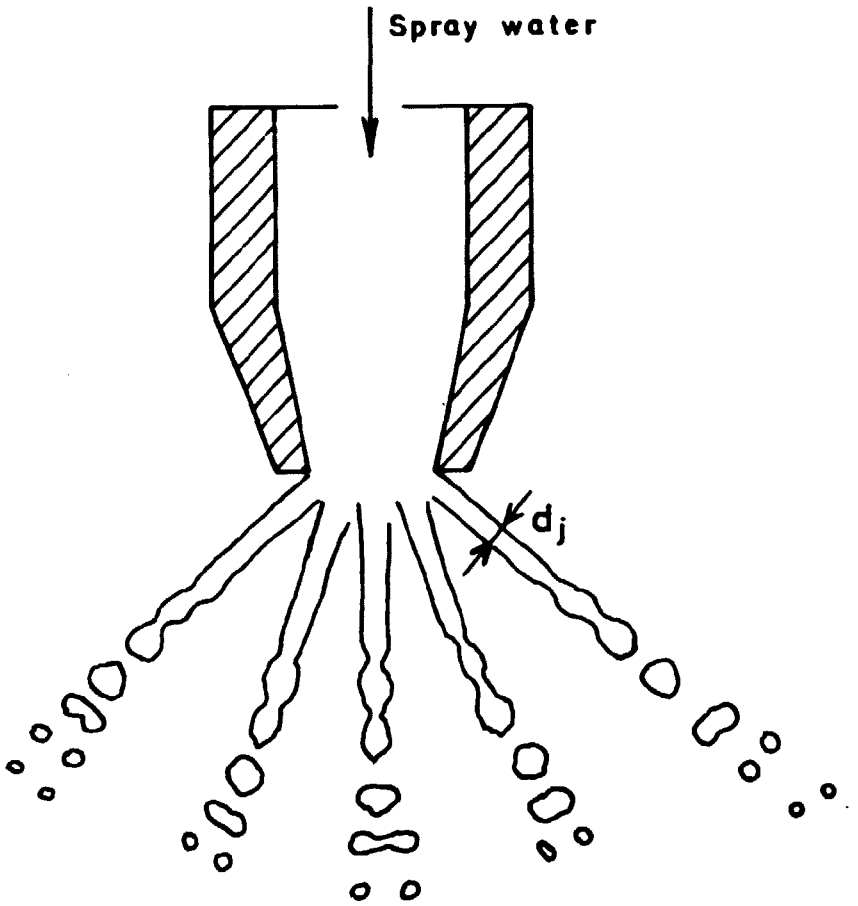

Fig. 3.2. Spray Nozzel Model

The droplets, produced from the jets, will be deformed due to the drag. Let P_o be the pressure distribution outside the droplet and P_s the pressure increment from the surface tension. For a droplet to be in equilibrium the pressure inside the droplet must be constant, i.e.

$$P_o + P_s = \text{constant} \tag{3.17}$$

Assuming the deformed droplet has the shape of an ellipsoid with rotational symmetry, the equilibrium deformation, cf. appendix A, is given by

$$\alpha^{\frac{1}{2}} + \alpha^{-\frac{5}{2}} - 2\alpha^2 = \min(0.5, C_D) \tag{3.18}$$

where

$$\alpha = \frac{d_d'}{d_d} \tag{3.20}$$

C_D is given by (3.9) and d_d' is the thickness of the droplet in the direction of motion. If the deformed droplet has to break up without additional work being done, the surface energy must be maintained. Assuming the droplet to break up into a set of spherical daughter-droplet, the number will be given by

$$n_d = \left\{ \frac{1}{2\alpha} + \sqrt{\alpha}\, \frac{\ln(\alpha^{-\frac{3}{2}} + \sqrt{\alpha^{-3}-1})}{2\sqrt{\alpha^{-3}-1}} \right\}^3 \tag{3.21}$$

These droplets may break up again if the Weber number is larger than 13.

A droplet can at least break up into two daughter droplets, and using a drag coefficient of 0.5 the critical Weber number can be determined from (3.18) and (3.21) to

$$We_c = 13.1 \tag{3.22}$$

This is in excellent agreement with experiments[2].

3.1.6. Counter Current Flow Limitation

Upward steam-flow will reduce the amount of spray water able to penetrate into the fuel element. In case of very large steam flow no liquid at all gets into the bundle. This phenomenon[2] is called Counter Current Flow Limitation, CCFL.

CCFL will occur either at the upper tie-plate or at one of the spacers where the cross section is smallest. However, as the steam flow will increase up through the bundle due to the evaporation, CCFL is most likely to occur at the upper tie plate.

A CCFL correlation for the upper tie-plate and the entrance to the by-pass channel is incorporated in CORECOOL. CCFL is mainly given as a balance between kinematic forces and gravity. A good correlation is given by Wallis[2]

$$\sqrt{j_g^*} + m\sqrt{j_\ell^*} = C \tag{3.23}$$

where

$$j_g^* = j_g \left\{ \frac{\rho_g}{g\, D_h (\rho_\ell - \rho_g)} \right\}^{\frac{1}{2}} \tag{3.24}$$

$$j_\ell^* = j_\ell \left\{ \frac{\rho_\ell}{g\, D_h (\rho_\ell - \rho_g)} \right\}^{\frac{1}{2}} \tag{3.25}$$

However, for large diameters the CCFL[6] tend to be independent of the diameter, and a better correlation is given by the Kutateladze number.

$$\sqrt{K_g} + m\sqrt{K_\ell} = C \tag{3.26}$$

where

$$K_g = \frac{j_g \sqrt{\rho_g}}{(\sigma \cdot g(\rho_\ell - \rho_g))^{1/4}} \tag{3.27}$$

$$K_\ell = \frac{j_\ell \sqrt{\rho_\ell}}{(\sigma \cdot g(\rho_\ell - \rho_g))^{1/4}} \tag{3.28}$$

In fig. 3.3 is given a plot of a set of runs with CORECOOL.

3.2. Energy Generation

Energy is generated due to the decay of fission products, and the metal-water reaction. Energy generation due to decay of fission prod-

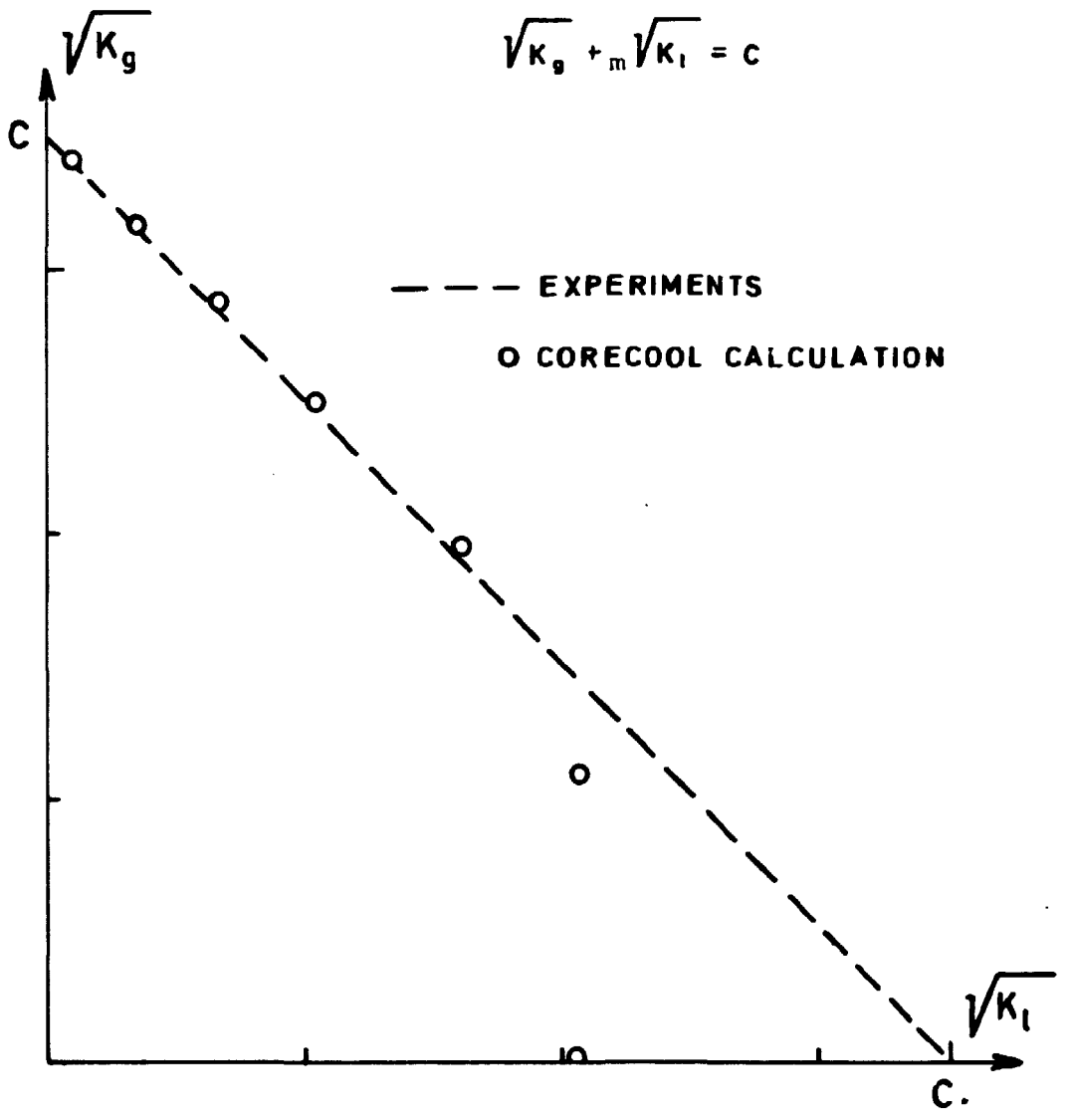
$\sqrt{K_g}$
$\sqrt{K_g} + m\sqrt{K_l} = C$
C
EXPERIMENTS
O CORECOOL CALCULATION
$\sqrt{K_l}$
C.

Fig.3.3.C C F L.

ucts is included in the fuel, and no decay heat or gammaheating is assumed to exist anywhere else. CORECOOL does not contain a fuel rod failure model and thus metal-water reactions is only included at the outside of the fuel rods. For water-rods and channel metal-water reactions are assumed to take place on either side.

3.2.1. Decay Heat

Energy generation from decay of fission products is calculated as a fraction of the power of the bundle just before the accident. The fraction is a function of the time.

$$Q_d''' = Q_o''' f(t) \tag{3.29}$$

f(t) is based on the history of the fuel element prior to the accident. In many cases the ANS-standard[7] is used.

3.2.2. Metal-Water Reaction

At high temperatures zirconium and steam will react chemically and energy will be produced[8].

$$Zr + 2\ H_2O \rightarrow Zr\ O_2 + 2\ H_2 + Q_M \tag{3.30}$$

$$Q_M = 6.669 \cdot 10^6 - 0.257 \cdot 10^3\ T \tag{3.31}$$

The reaction rate is determined by the diffusion of steam through the $Zr\ O_2$ layer at the surface, and a parabolic law exists

$$\frac{ds}{dt} = \frac{K}{s} \exp\left(\frac{-\Delta E}{R(T+273{\cdot}15)}\right) \tag{3.32}$$

For zirconium

$K = 3.937 \cdot 10^{-5}\ m^2/s$
$\Delta E = 1.905 \cdot 10^5\ J/mole$
$R = 8.318\ J/mole\ ^oC$

In accordance with appendix K[9] the metal-water reaction is not assumed to be steam-limited, which is only the case for very high temperatures, and when very small amounts of spray water is available.

3.3. Conduction and Convection Heat Transfer

Heat transfer due to conduction or convection are important mechanisms in the heat transfer from the fuel rods and the channel to the two-phase flow and in the interfacial heat and mass transfer.

Conduction heat transfer is important for the heat transfer in the droplets and the films. The steam-water interface will be at saturation temperature, and if the liquid in the droplets or the films is subcooled or superheated conduction heat transfer will exist.

Convection heat transfer will be important for the steam. It will exist between the fuel rods or the channel and the steam, and if the steam is superheated from the steam to steam-water interfaces. Convection heat transfer will also exist as boiling heat transfer in sputtering fronts and in the lower plenum owing to the large heat capacity of the vessel wall and the guide tubes.

3.3.1. Conduction Heat Transfer in Droplets and Films

If there is a difference between the bulk temperature and the surface temperature of a droplet or a film conduction heat transfer will take place.

For the droplets an asymptotic solution to the heat conduction equation is used, cf. appendix B, and the surface heat flux becomes

$$q''_{\ell g} = \frac{2}{3}\pi^2 \frac{k_\ell}{d_d}(T_d - T_s) \tag{3.33}$$

In the case of a falling film a linear temperature profile is assumed and the surface heat flux becomes

$$q''_{\ell g} = \frac{2\,k_\ell}{s_f}(T_f - T_s) \tag{3.34}$$

3.3.2. Convection Heat Transfer between Super-heated Steam and Droplets

Due to the steam superheat there will be a temperature difference between the steam and the interface between the steam and the droplets, and thus also a net heat transfer. The heat transfer will be both convection and radiation, the latter, however, will be considered in section 3.4, and only convection will be treated here. Numerous correlations are given in the litterature[10] and a good overall correlation is[10]

$$\beta = Nu_d \, k_g \, n_d \, \pi \, d_d \tag{3.35}$$

$$Nu_d = 3.20 + 0.75 \cdot Re_d^{0.5} \cdot Pr_g^{0.33} \tag{3.36}$$

$$Re_d = \frac{d_d \, \rho_g |u_g - u_d|}{\mu_g} \tag{3.37}$$

The correlation 3.36 does not approach 2.0 for $Re_d \to 0$, but is the best overall fit for typical Re_d around 10^3.

3.3.3. Convection Heat Transfer from a Surface to Superheated Steam

The presence of droplet in a steam atmosphere has two effects on the convection wall to steam heat transfer. The bulk steam temperature will be lowered toward the saturation temperature, increasing the heat transfer. And secondly the temperature profile of the steam will be changed causing a steeper temperature gradient close to the wall. This effect will also enhance the heat transfer. The single phase heat transfer coefficient will be given by

$$Nu_{g,s} = \begin{cases} 3.316 + 0.895 \, \frac{p}{d_r} & \text{for laminar flow}^{11)} \qquad (3.38) \\ 0.023 \, Re_g^{0.8} \, Pr_g^{0.4} & \text{for turbulent flow}^{12)} \qquad (3.39) \end{cases}$$

In reference 13) Sun, Gonzalez and Tien solves the continuity and energy equation for the temperature profile of the steam, and if a parabolic velocity profile for the steam is assumed, one obtains

$$Nu_g = \frac{2x \, I_1(x)}{I_0(x) - \frac{8}{x^2} I_2(x)} \tag{3.40}$$

$$x = \frac{D_h}{2} \sqrt{\frac{\beta \, h_g}{k_g \, h_{\ell_g}}} \tag{3.41}$$

However, (3.40) is derived due to the assumption that the temperature profile of the steam is determined from a balance between heat transfer from the wall and heat transfer to the droplets, and the terms $\frac{\partial}{\partial z}$ are neglected in the continuity and energy equations. This is valid only for large droplet concentrations, for zero droplet concentration the single phase Nusselts number for a tube is 4.36, whereas the limiting value of (3.40) is 6.0.

For large droplet concentration an asymptotic approximation to (3.40) is

$$Nu_g \to 2x - 1 \quad \text{for } x \to \infty \tag{3.42}$$

An expression having this behaviour, and fulfilling (3.38) or (3.39) for x=0 is given by

$$Nu_g = 2x - 1 + \frac{(Nu_{g,s} + 1)^2}{Nu_{g,s} + 1 + 2x} \tag{3.43}$$

Here the auxiliary criteria of zero slope for x=0 is used, and from (3.35), (3.41) and (3.43) it is seen that Nu_g increases linearity with n_d for small n_d.

In fig. 3.4 is given a plot of (3.40) and (3.43).

3.3.4. Convection Heat Transfer from a Surface to Falling Film

In case a surface is covered with a falling film, upstream of the front, where nucleate boiling may occur, a constant heat transfer coefficient may be used. The heat transfer coefficient may be set to a value[14,15] of

$$h_f = 3.0 \cdot 10^3 - 5.0 \cdot 10^3 \text{ W/m } ^\circ\text{C}. \tag{3.44}$$

3.3.5. Sputtering Heat Transfer

The movement of the film front on rods and channel is determined as a balance between heat conduction and convection. Energy is removed from the hot unwetted part of the rods or the channel by axial and radial conduction, and then from the wetted part by nucleate boiling transferred to the film, cf. fig. 3.5.

Assuming a constant heat transfer coefficient for the wetted part of the surface, the two-dimensional heat conduction problem has been solved by many authors[16,17,18]. Andersen obtained the following asymptotic expressions

$$\left\{Pe\theta^{(1-\frac{\sqrt{\pi}}{2})}\right\} = \left\{Bi\theta^{-\sqrt{\pi}}\right\}0.5 \tag{3.45}$$

$$\text{for } Bi \cdot \theta^{-\sqrt{\pi}} < 2^{\frac{\sqrt{\pi}}{2}}$$

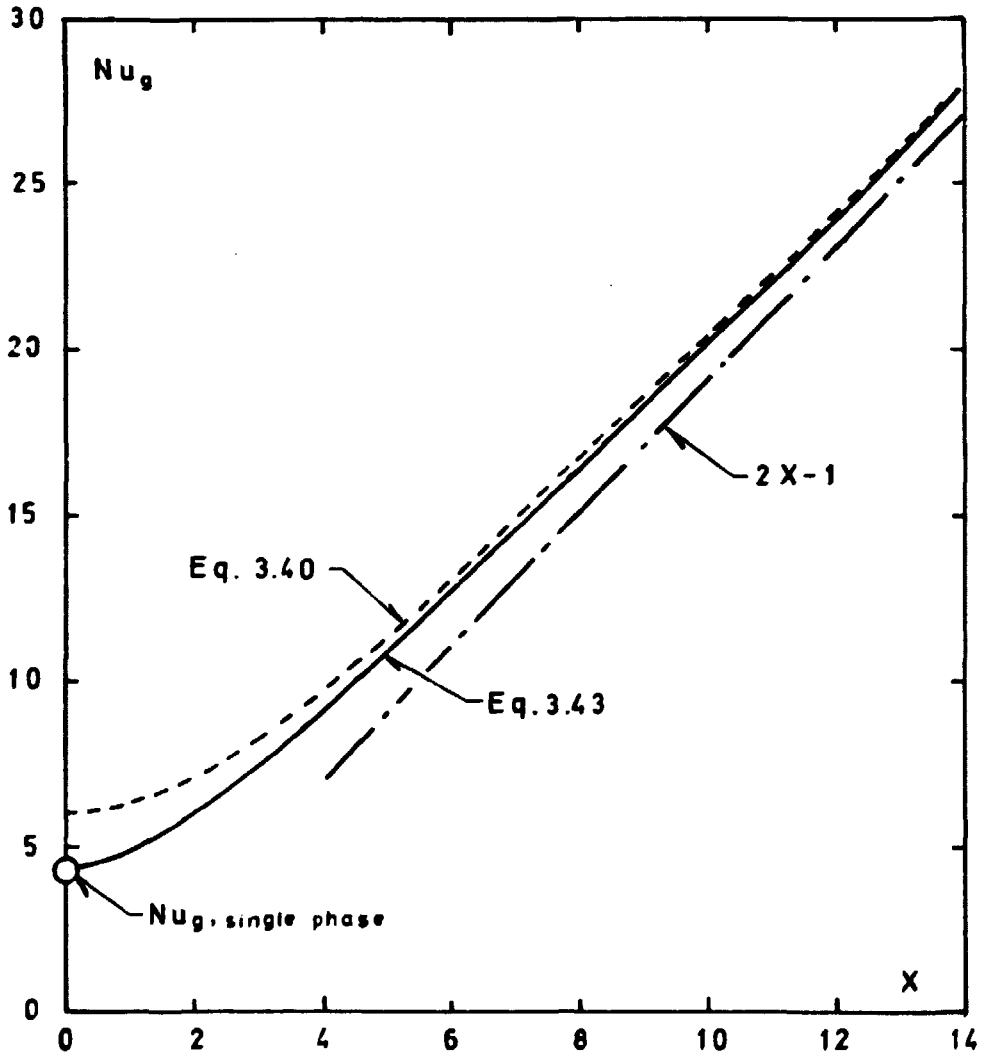

Fig. 3.4. Nusselts Number for a steam - droplet mixture.

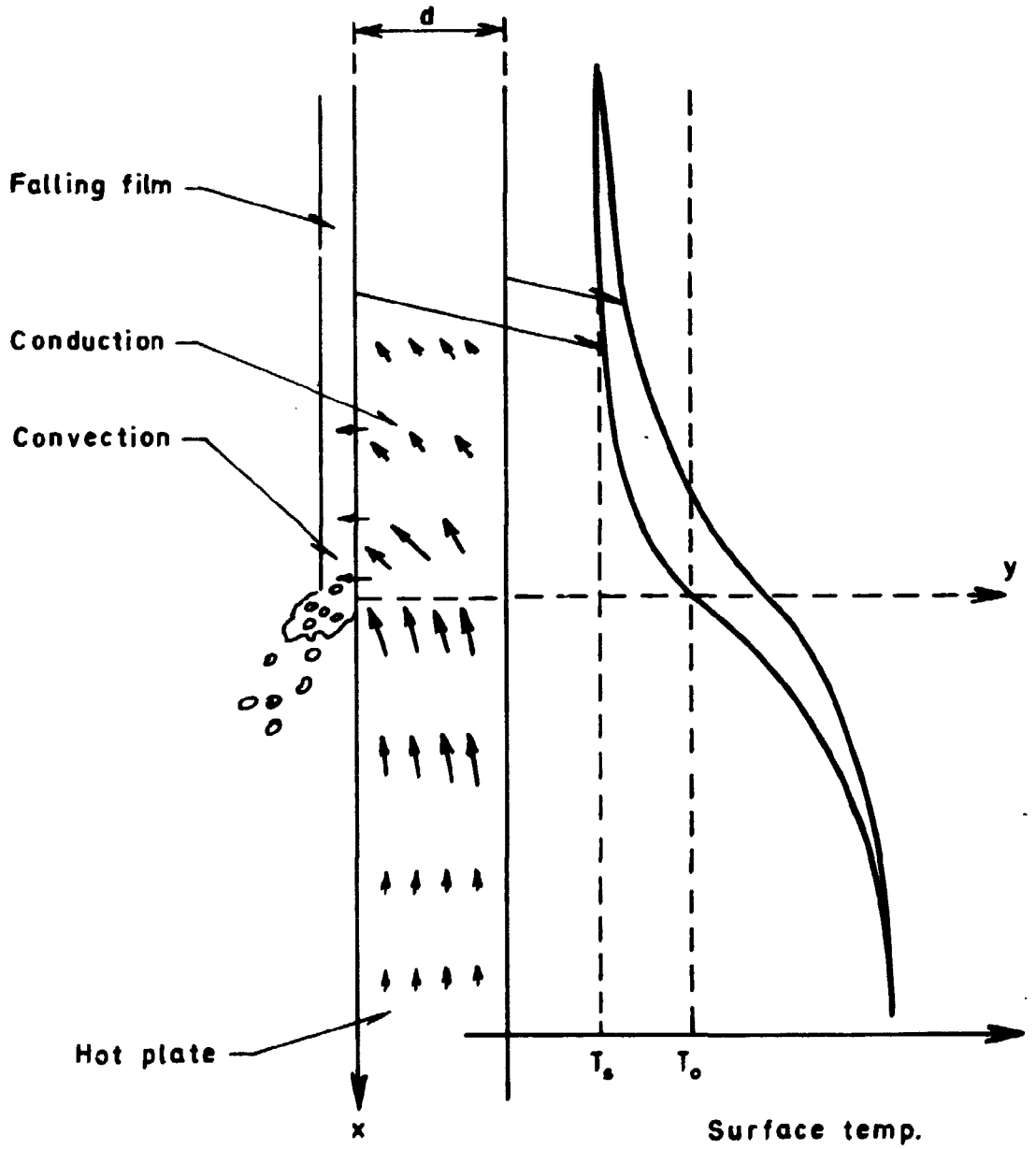

Fig. 3.5. Physical phenomena in rewetting

$$\left\{Pe\theta^{(1-\frac{\sqrt{\pi}}{2})}\right\} = 2^{-\frac{\sqrt{\pi}}{2}} \cdot \left\{Bi\cdot\theta^{-\sqrt{\pi}}\right\} \qquad (3.46)$$

$$\text{for } 2\,\frac{\sqrt{\pi}}{2} \leq Bi\theta^{-\sqrt{\pi}}$$

A good overall correlation was found to

$$\left\{Pe\theta^{(1-\frac{\sqrt{\pi}}{2})}\right\} = \left\{(Bi\theta^{-\sqrt{\pi}})^{1.5} + 2^{-\frac{3}{4}\sqrt{\pi}}(Bi\theta^{-\sqrt{\pi}})^{3}\right\}^{\frac{1}{3}} \qquad (3.47)$$

where

$$Pe = \frac{\rho_w\, c_w\, u_{fr}\, d_w}{k_w} \qquad (3.48)$$

$$Bi = \frac{h_{fr}\, d_w}{k_w} \qquad (3.49)$$

$$\theta = \left\{\frac{(T_\infty - T_s)(T_\infty - T_o)}{(T_o - T_s)^2}\right\}^{\frac{1}{2}} \qquad (3.50)$$

In fig. 3.6 is shown the result of the solution to the heat conduction problem by a finite difference method, and in fig. 3.7 is shown the result of a correlation of (3.47) against the data of Bennet et al.[19] and the low spray flow data of Duffey and Porthouse[20]. Using a least square method the best values for h_{fr} and T_o were found to

$$h_{fr} = 1.13\cdot10^6 \text{ W/m}^2\,^\circ\text{C} \qquad (3.51)$$

$$T_o = T_s + 65^\circ\text{C} \qquad (3.52)$$

3.3.6. Gas Gap Heat Transfer

The heat transfer across the gas gap between the fuel and the cladding is a combination of heat transfer due to physical contact between the fuel and the cladding, thermal conduction through the gas, and thermal radiation. The conduction heat transfer in the gas is a function of the composition of the gas, and the history of the fuel.

Accordingly a general model is difficult to make, and in CORECOOL, the heat transfer coefficient is calculated by

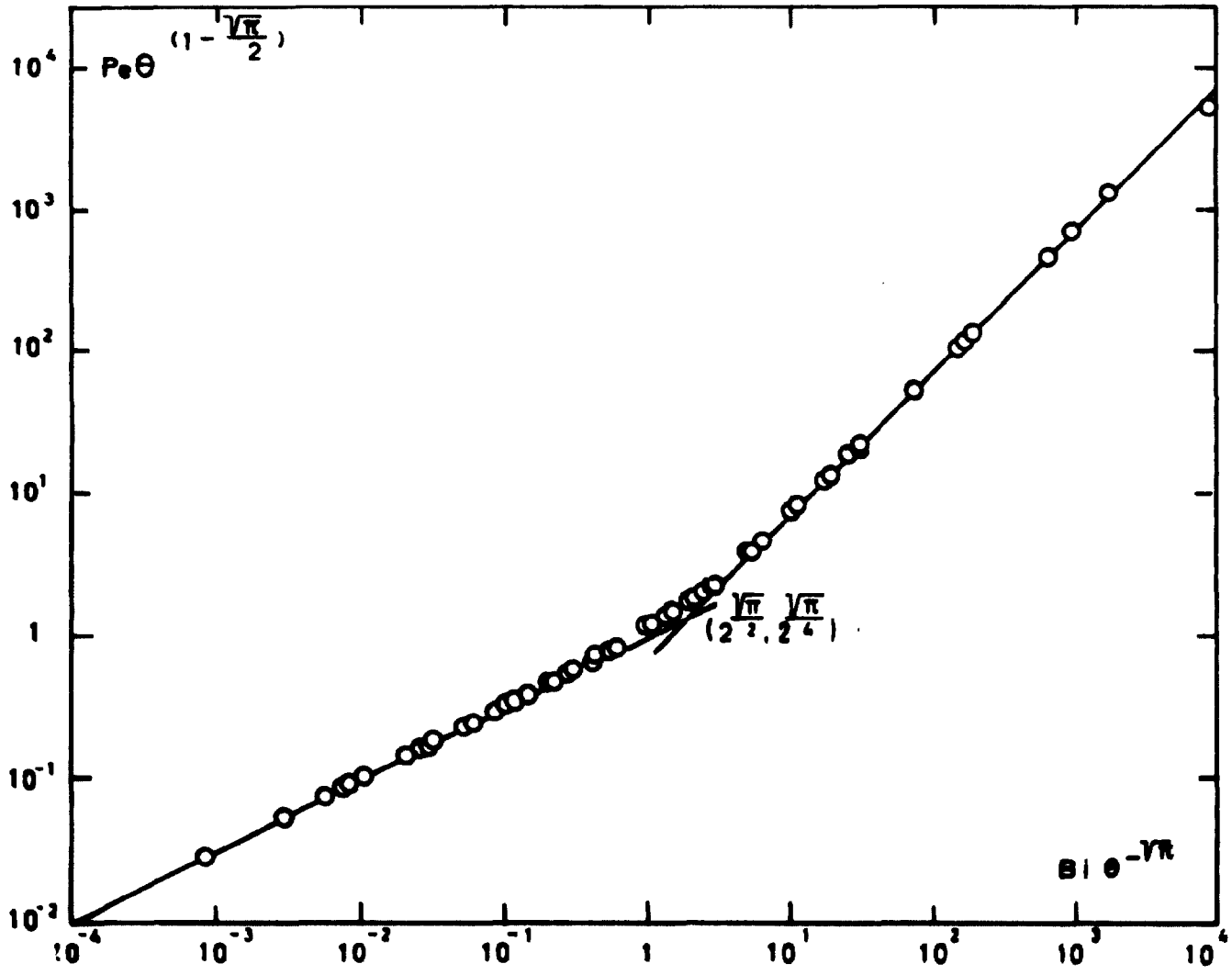

Fig. 3.6. Rewetting rate as function of modified Biot number, result of the finite difference method.

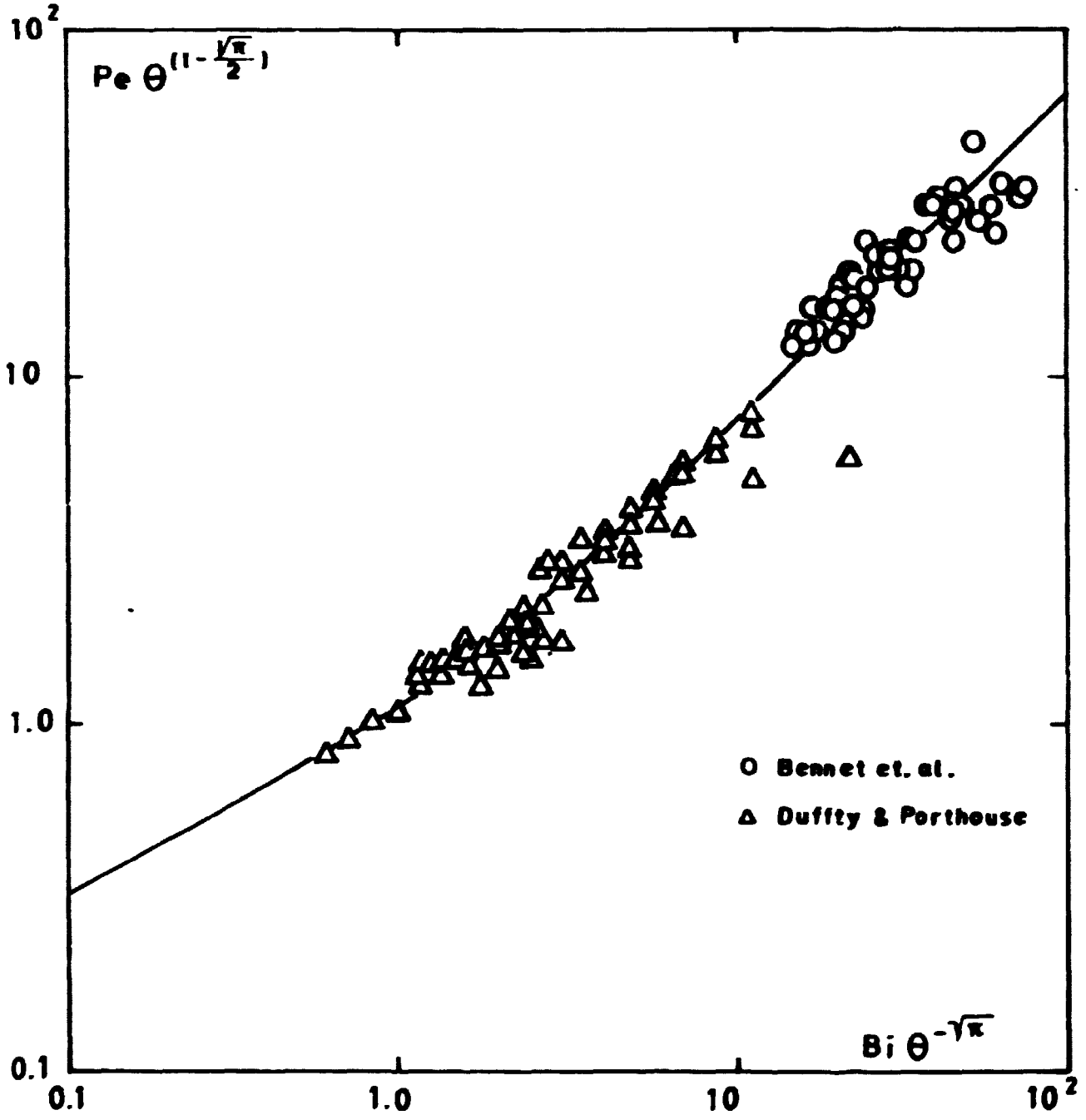

Fig. 3.7. Comparison of theory with experiments, modified Peclet-number versus modified Biot-number

$$h_{gap} = \frac{k_{gap}}{d_{gap}} \quad . \tag{3.53}$$

3.3.7. Heat Transfer in the Lower Plenum

In the lower plenum heat is transferred from the vessel and the guide tubes to the two phase mixture, which is assumed to exist as a pool of water and a steam-droplet mixture above it.

Heat transfer is only to the liquid and the Rohsenow[21] pool boiling heat transfer correlation is used

$$\frac{c_\ell (T_w - T_s)}{h_{\ell g}} = 0.013 \left\{ \frac{q''_w}{\mu_\ell h_{\ell g}} \sqrt{\frac{\sigma}{g(\rho_\ell - \rho_g)}} \right\}^{0.33} Pr_\ell^{1.7} \tag{3.54}$$

A simple flashing correlation is included in the case the liquid is superheated.

$$\Phi_{\ell g,flash} = \frac{c_p (T_\ell - T_s)\rho_\ell}{h_{\ell g}\, \tau_{flash}} \quad . \tag{3.55}$$

3.4. Radiation Heat Transfer

The model for radiation heat transfer, which is the other important heat transfer mechanism, include surface to surface radiation and radiation to the two-phase mixture in the bundle. The surface to surface radiation is calculated using the transport corrected[22] radiation model extended to include a participating medium in the enclosure. The model for the two-phase mixture includes emission and absorption of thermal radiation and is based on the semi grey radiation model.

3.4.1. The Basic Radiation Model

The model for radiation heat transfer is based on the following assumptions:

1. All surfaces are grey and diffuse.
2. All surfaces emit radiation uniformly.
3. Of the reflected radiation from a surface a fraction (1-μ) is reflected isotropically and the rest μ is reflected backward toward the origin of the incident radiation.

4. The steam absorbs and emits radiation, but direct radiation from the steam to the droplets is neglected.

5. The droplets absorb radiation, but neither emit nor reflect radiation.

6. Uniform temperature distribution of the steam and droplets.

7. Semigrey radiation model.

The assumption of no direct radiation from the steam to the droplets, and that scattering can be neglected for the droplets is consistent with the optical thin limit approximation[13], and the assumption that the droplets do not emit radiation is justified by their low temperature.

The optical thickness based on the Planck mean absorption coefficient for steam and the peak value of the principal 2.7 μ band for typical ECCS transients is about 0.2 to o.3, in which case the optical thin limit approach gives good results. If however, the droplet concentration is large, the medium is not optical thin, but in that case the steam superheat is low and the assumption of uniform temperatures of the steam and liquid is good. Owing to the low temperatures of either phase in this case there will be no radiation heat transfer direct between the phases, and the model, which is derived from the two flux model, see Appendix C, is still good. The volume fraction of droplets for ECCS transients are typically around 0.01. For a typical droplet size of $1.9 \cdot 10^{-3}$ m, a steam temperature of 500°C, and a pressure of 1 bar, the optical thickness for an 8X8 bundle is, in Table 1, given for various values of the droplet concentration.

α_I droplet conc.	a_g m^{-1}		a_ℓ m^{-1}	(a_g+a_ℓ) m^{-1}	Optical Thickness	
	Planck mean	Peak value			Planck mean	Peak value
5.10^{-3}	10.3	14.5	2.9	13.2	0.17	0.23
10^{-2}	10.3	14.5	5.8	16.1	0.21	0.26
2.10^{-2}	10.3	14.5	11.7	22.0	.0.29	0.34
5.10^{-2}	10.3	14.5	29.2	39.5	0.52	0.57

Table 3.1. Typical values for the optical thickness for a fuel bundle.

The radiosity of a surface is given by, cf. fig. 3.8

$$B_i = \varepsilon_i S_i + (1-\varepsilon_i)H_i \tag{3.56}$$

where

$$S_i = \sigma T_i^4 \tag{3.57}$$

$$H_i = \sum_j H_{ji} \tag{3.58}$$

and H_{ji} is the incident radiation coming from the direction of the j'th surface. The isotropic part of the radiosity is given by

$$B_i^I = \varepsilon_i S_i + (1-\mu_i)(1-\varepsilon_i)H_i \tag{3.59}$$

and the anisotropic part leaving in the direction of the j'th surface is given by

$$B_{ij}^A = \mu_i(1-\varepsilon_i)H_{ij} \tag{3.60}$$

The incident radiation from the direction of the j'th surface is the sum of the radiation leaving the j'th surface in the direction of the i'th surface reduced by the transmissivity of the medium plus what is emitted by the medium

$$H_{ji} = \frac{1}{A_i}(A_j B_j^I F_{ji} + A_j B_{ji}^A)\tau_{ji} + \varepsilon_{g_{ij}} F_{ij} S_g \tag{3.61}$$

where

$$\tau_{ij} = \tau_{ji} = e^{-R_{ij}(a_\ell + a_g)} \tag{3.62}$$

$$\varepsilon_{g_{ij}} = \frac{a_g}{a_\ell + a_g}(1-\tau_{ij}) \tag{3.63}$$

$$S_g = \sigma T_g^4 \tag{3.64}$$

R_{ij} is the beam length between surface i and surface j.

In agreement with the semigrey radiation model the absorption coefficients in the transmissivity, equation 3.62, is a function of the wall temperature, i.e. the temperature of the absorbed radiation,

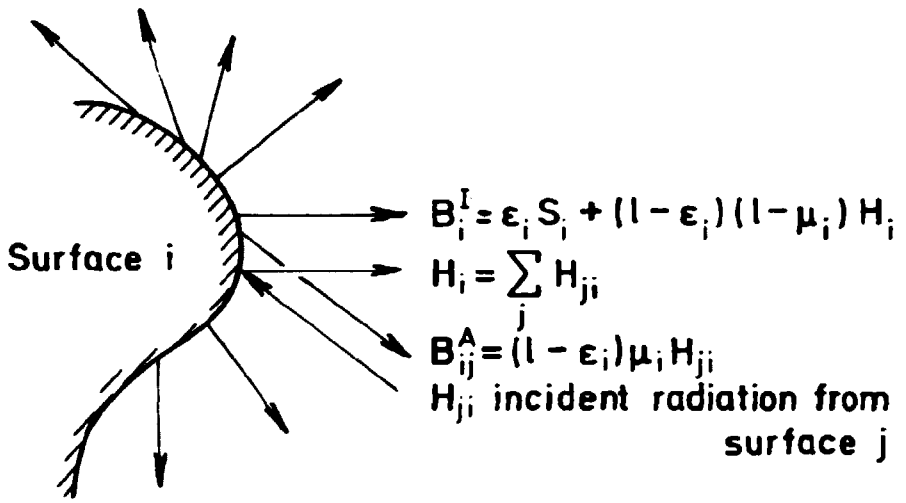

Fig. 3.8 Radiosity of a surface

whereas the emissivity, equation 3.63, is a function of the temperature of the medium, i.e. the emitted radiation.

Inserting equation 3.61 in 3.60 gives

$$A_i B^A_{ij} = \mu_i(1-\varepsilon_i)\{(A_j B^I_j F_{ji} + A_j B^A_{ji})\tau_{ji} + \varepsilon_{g_{ij}} A_i F_{ij} S_g\} \quad (3.65)$$

By changing the subscripts in equation (3.65) we can eliminate B_{ji} and obtain

$$B^A_{ij} = \frac{\mu_i(1-\varepsilon_i)\{(B^I_j+\mu_i(1-\varepsilon_j)B^I_i\tau_{ij})\tau_{ij}+\varepsilon_{g_{ij}}S_g(1+\mu_j(1-\varepsilon_j)\tau_{ij})\}}{1-\mu_i(1-\varepsilon_i)\mu_j(1-\varepsilon_j)\tau^2_{ij}} F_{ij} \quad (3.66)$$

Combining equation 3.56, 3.58, 3.60 and 3.66 we obtain

$$B^I_i = \varepsilon_i S_i + (1-\mu_i)(1-\varepsilon_i)\sum_i \frac{(B^I_j+\mu_j(1-\varepsilon_j)B^I_i\tau_{ij})\tau_{ij}+\varepsilon_{g_{ij}}S_g(1+\mu_j(1-\varepsilon_j)\tau_{ij}))}{1-\mu_i(1-\varepsilon_i)\mu_j(1-\varepsilon_j)\tau^2_{ij}} F_{ij} \quad (3.67)$$

This is a system of linear equation and it can be solved for the isotropical radiosities by standard methods.

The net heat flux at surface i is then, using (3.56) and (3.59), found to

$$Q_i = A_i(B_i - H_i) = \frac{A_i\varepsilon_i}{1-\varepsilon_i}\frac{S_i(1-\mu_i(1-\varepsilon_i))-B^I_i}{1-\mu_i} \quad (3.68)$$

The net energy absorbtion in the droplets is given by

$$Q_\ell = \sum_i A_i \sum_j (B^I_i F_{ij} + B^A_{ij})\varepsilon_{\ell_{ij}}$$

$$= \sum_i A_i \sum_j \frac{B^I_i+\mu_i(1-\varepsilon_i)\{B^I_j\tau_{ij}+\varepsilon_{g_{ij}}S_g(1+\mu_j(1-\varepsilon_j)\tau_{ij})\}}{1-\mu_i(1-\varepsilon_i)\mu_j(1-\varepsilon_j)\tau^2_{ij}} \varepsilon_{\ell_{ij}} F_{ij} \quad (3.69)$$

where

$$\varepsilon_{\ell_{ij}} = \frac{a_\ell}{a_\ell + a_g}(1 - \tau_{ij}) \quad (3.70)$$

and as energy must be conserved the net interchange of energy with the steam is given by

$$Q_g = \sum_i Q_i - Q_\ell \quad (3.71)$$

In fig. 3.9 is shown the electrical analog corresponding to equation 3.67, 3.68, 3.69 and 3.71. Note that $B^I/(1-\mu_i(1-\varepsilon_i))$ is not the total radiosity of surface i, but a kind of effective total radiosity. A rearrangement of equation 3.67 gives

$$0 = \left\{S_i - \frac{B_i^I}{1-\mu_i(1-\varepsilon_i)}\right\} \frac{A_i\varepsilon_i(1-\mu_i(1-\varepsilon_i))}{(1-\varepsilon_i)(1-\mu_i)}$$

$$+ \sum_j \left\{\frac{B_j^I}{1-\mu_j(1-\varepsilon_j)} - \frac{B_i^I}{1-\mu_i(1-\varepsilon_i)}\right\} \frac{A_i(1-\mu_i(1-\varepsilon_i))(1-\mu_j(1-\varepsilon_j))\tau_{ij}F_{ij}}{1-\mu_i(1-\varepsilon_i)\mu_j(1-\varepsilon_j)\tau_{ij}^2}$$

$$+ \left\{S_g - \frac{B_i^I}{1-\mu_i(1-\varepsilon_i)}\right\} \sum_j \varepsilon_{g_{ij}} \frac{A_i(1-\mu_i(1-\varepsilon_i))(1+\mu_j(1-\varepsilon_j)\tau_{ij})F_{ij}}{1-\mu_i(1-\varepsilon_i)\mu_j(1-\varepsilon_j)\tau_{ij}^2}$$

$$+ \left\{S_\ell - \frac{B_i^I}{1-\mu_i(1-\varepsilon_i)}\right\} \sum_j \varepsilon_{\ell_{ij}} \frac{A_i(1-\mu_i(1-\varepsilon_i))(1+\mu_j(1-\varepsilon_j)\tau_{ij})F_{ij}}{1-\mu_i(1-\varepsilon_i)\mu_j(1-\varepsilon_j)\tau_{ij}^2} \qquad (3.72)$$

and rearrangement of equation 3.69 gives

$$Q_\ell = \sum_i \left\{\frac{B_i^I}{1-\mu_i(1-\varepsilon_i)} - 0\right\} \sum_j \varepsilon_{\ell_{ij}} \frac{A_i(1-\mu_i(1-\varepsilon_i))(1+\mu_j(1-\varepsilon_j)\tau_{ij})F_{ij}}{1-\mu_i(1-\varepsilon_i)\mu_j(1-\varepsilon_j)\tau_{ij}^2}$$

$$+ \left\{S_g - 0\right\} \sum_i \sum_j \varepsilon_{\ell_{ij}} \varepsilon_{g_{ij}} \frac{A_i\mu_i(1-\varepsilon_i)(1+\mu_j(1-\varepsilon_j)\tau_{ij})F_{ij}}{1-\mu_i(1-\varepsilon_i)\mu_j(1-\varepsilon_j)\tau_{ij}^2} \qquad (3.73)$$

The viewfactors and the beam lengths are dependent on the geometry only and given by the general expressions[27], cf. fig. 3.10

$$F_{ij} = \frac{\int_{A_i}\int_{A_j} \frac{\cos\beta_i \cos\beta_j}{\pi R^2} dA_j\, dA_i}{A_i} \qquad (3.74)$$

$$R_{ij} = \frac{\int_{A_i}\int_{A_j} \frac{\cos\beta_i \cos\beta_j}{\pi R} dA_j\, dA_i}{A_i F_{ij}} \qquad (3.75)$$

For elongated surfaces, as radiation in the axial direction is neglected, (3.74) reduces to the crossed string method.

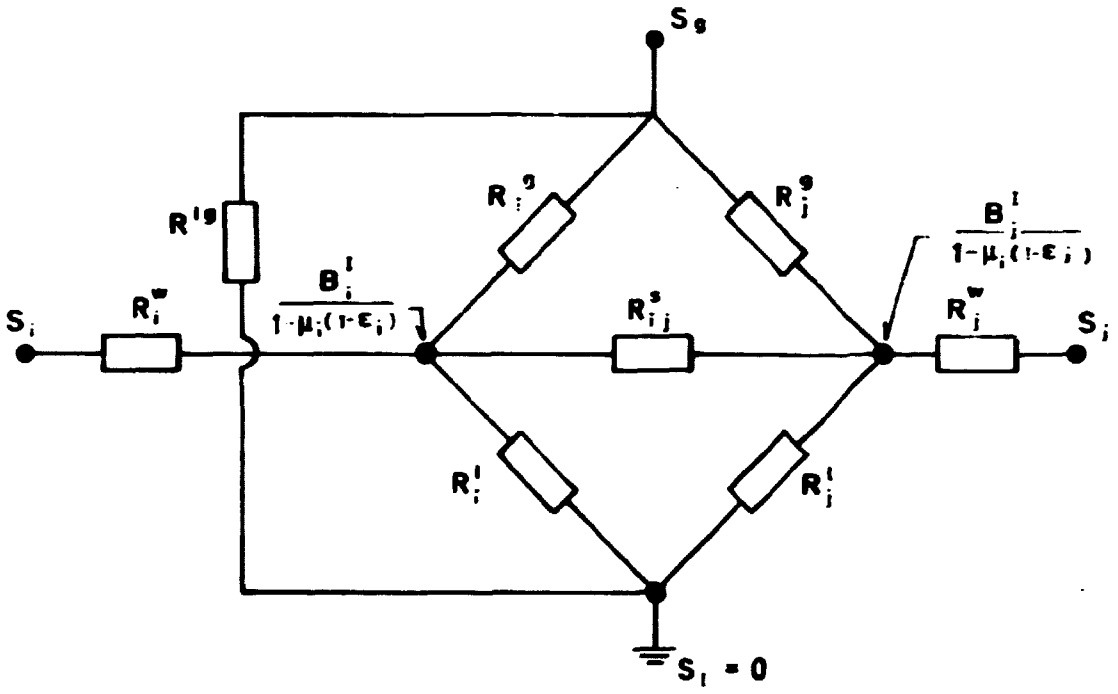

Fig. 3.9. Electrical analog for radiation model.

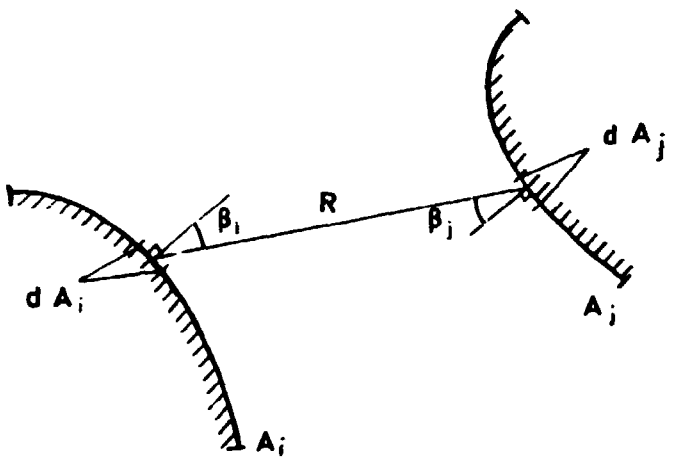

Fig.3.10. Radiation heat transfer between two surfaces.

3.4.2. Radiation Properties of Steam and Droplets

The interaction of thermal radiation with the steam and droplets is based on the semigrey radiation model, and the assumption that the medium is optical thin.

For the droplets it can be shown[13], that, when the medium is optical thin, scattering can be neglected and the absorption coefficient will be given by[13]

$$a_\ell = 1.11 \cdot \frac{1-\alpha}{d_d} \tag{3.76}$$

For absorption of thermal radiation between surface i and surface j the mean void fraction between the void just outside surface i and j respectively is used.

The absorption coefficient for the steam is a function of the temperature and the pressure and varies as shown in fig. 3.11[23]. A good polynomial fit is given by

$$a_g = P\{5.2\cdot10^{-4} + -9.0\cdot10^{-7}\cdot T + 5.6\cdot10^{-10}\cdot T^2 - 1.2\cdot10^{-13}\cdot T^3\} \tag{3.77}$$

3.4.3. Anisotropical Reflection

Use of view factors and standard methods without correction[26] for anisotropical reflection requires that the radiosity is constant over the surface elements. With constant temperature for each surface element the emitted radiation from the surface will be uniform, but as the incident radiation generally is not uniformly distributed over the surface element neither the reflected radiation nor the radiosity will be uniform. However, no matter how the distribution of the reflected radiation is, we can always split it into an isotropical part and a non-isotropical part.

Let $I_e(\phi)$ be the distribution function of the emitted radiation from a surface with uniform temperature, cf. fig. 3.12

$$\int_0^{2\pi} I_e(\phi)d\phi = 1 \tag{3.78}$$

and $I_r(\phi)$ the distribution function of reflected radiation coming from the direction $\phi = 0$, cf. fig. 3.12

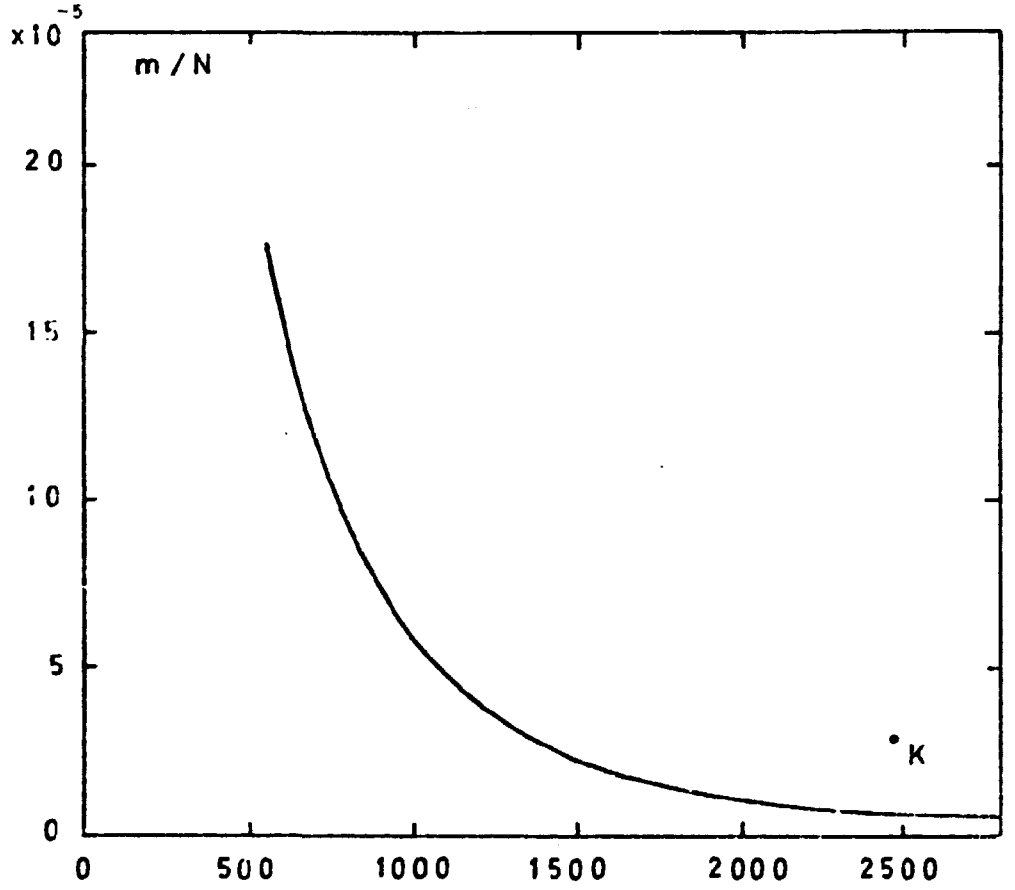

Fig. 3.11. Planck mean absorption coefficient for steam

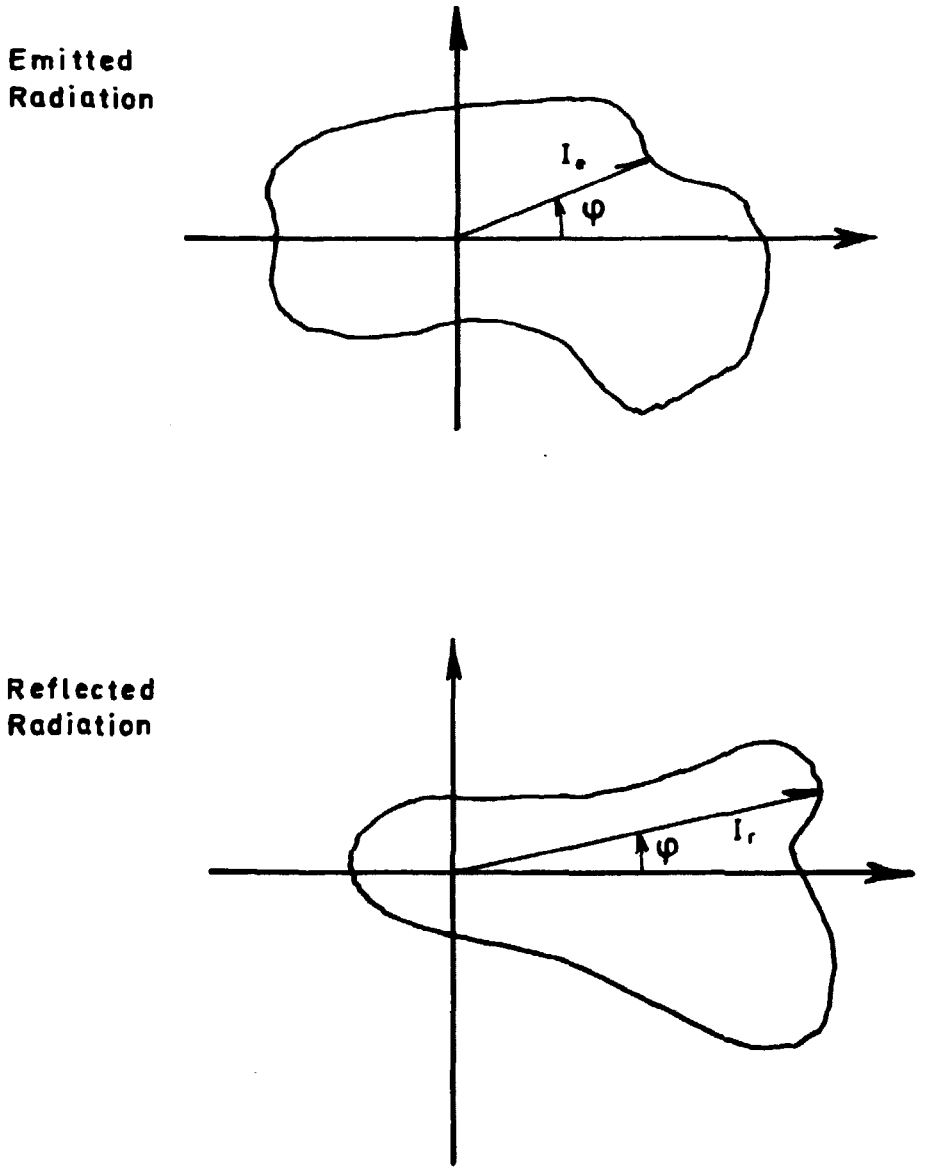

Fig. 3.12. Distribution Functions for Emitted and Reflected Radiation From a Surface

$$\int_0^{2\pi} I_r(\phi)d\phi = 1 \tag{3.79}$$

Note that $I_e(\phi)$ is necessarily not a constant, e.g. large and curved surfaces.

If the incident radiation was uniformly distributed over the surface the reflection in the direction (ϕ) should be $I_e(\phi)$.

The anisotropical part of the reflected radiation is given by

$$I_a(\phi) = I_r(\phi) - I_e(\phi) \tag{3.80}$$

From the anisotropical reflected radiation in the direction ϕ, the flux in the direction $\phi = 0$ is

$$I_a(\phi)\cos(\phi)$$

Integrating over all directions we obtain the fraction of the reflected radiation which is anisotropical reflected backwards in the direction opposite to the incident radiation

$$\mu = \int_0^{2\pi} (I_r(\phi) - I_e(\phi))\cos(\phi)d\phi \tag{3.81}$$

As the tendency for diffuse surfaces is to reflect the radiation backward toward the origin of the incident radiation, $\mu \geq 0$, and similarily as at most all the radiation can be reflected backwards, $\mu \leq 1$ and thus

$$0 \leq \mu \leq 1 \tag{3.82}$$

Eks. 1: Cylindrical rod.

Owing to the symmetry it is easily seen that

$$I_e(\phi) = \frac{1}{2\pi}$$

The intensity of the reflected radiation in the direction of ϕ is given by

$$I_r = (1 + \cos(\phi))k$$

Using (3.79) we get

$$I_r(\phi) = \frac{1}{2\pi}\{1 + \cos(\phi)\}$$

From (3.81) we get

$$\mu = \frac{1}{2\pi}\int_0^{2\pi} \cos^2(\phi)d\phi = \frac{1}{2}$$

Eks. 2: Inside of a large rectangular or cylindrical channel.

Owing to the symmetry we get

$$I_e(\phi) = \frac{1}{2\pi}$$

If the incident radiation is uniformly distributed over the surface, then $I_r = I_e$ and we get $\mu = 0$. However, if the source of incident radiation is close to the channel wall, and of such a nature that the main part of the radiation hits such a small area that the channel can be considered plane, then

$$I_r(\phi) = \begin{cases} \frac{1}{2}\cos(\phi) & -\frac{\pi}{2} < \phi < \frac{\pi}{2} \\ 0 & \text{else} \end{cases}$$

and we obtain

$$\mu = \int_0^{2\pi} \frac{1}{2}\cos^2(\phi)d\phi = \frac{\pi}{4}$$

In table 3.2 is given a comparison of the black body radiation calculated with an "exact" method, the transport corrected method and the standard method with two surfaces for the outer rods for a 7 rod cluster as shown in fig. 3.13. The power distribution of the rods was uniform and the channel kept cold. And in order to make the calculation of the view factors easy the ratio of the pitch to the rod diameter was chosen to $\frac{\sqrt{3}}{2}$.

As it is seen from the table the transport corrected method gives a significant improvement from the standard method.

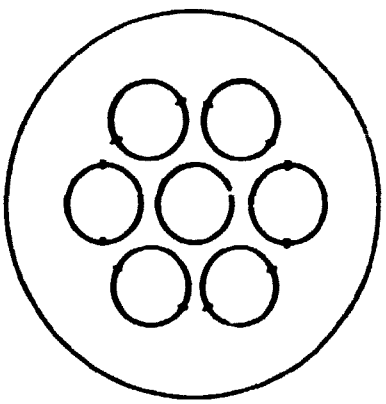

Fig.3.13. 7-rod cluster

ε	Exact	Transport correction		Standard
		$\mu_r = 0.3$ $\mu_c = 0$	$\mu_r = 0.5$ $\mu_c = 0.5$	
0.1	29.1	26.5	28.3	25.6
	26.4	25.2	26.3	24.8
0.3	10.8	9.50	10.6	8.81
	8.96	8.33	9.00	8.03
0.5	6.59	5.91	6.57	5.45
	5.20	4.88	5.28	4.67
0.7	4.58	4.27	4.61	4.02
	3.50	3.35	3.56	3.24
0.9	3.38	3.30	3.39	3.22
	2.51	2.47	2.53	2.44

Table 3.2. Comparison of black body radiation of center and outer rods for a 7-rod cluster.

3.5. Two Region Steam Temperature Model

Large steam superheat will exist in a fuel bundle during a core heat-up transient and large variations in the steam temperatures will exist. In the central region of the bundle a steam superheat of more than 500°C is very likely. On the other hand at the channel wall, the steam temperature will drop to the channel temperature. Accordingly the use of a uniform steam temperature[1)] across the bundle will lead to errors.

A typical temperature distribution is shown in Fig. 3.14. The heat transfer from the fuel rods to the two-phase flow will be over predicted in the central region of the bundle leading to too low fuel temperatures, and the heat transfer will be under predicted in the peripheral region leading to two high temperatures for the fuel.

3.5.1. The Model

The model for different steam temperatures in the two regions is based on the following assumptions

A high uniform superheat will exist in the central region and the temperature will drop linearily to the channel temperature across the peripheral region.

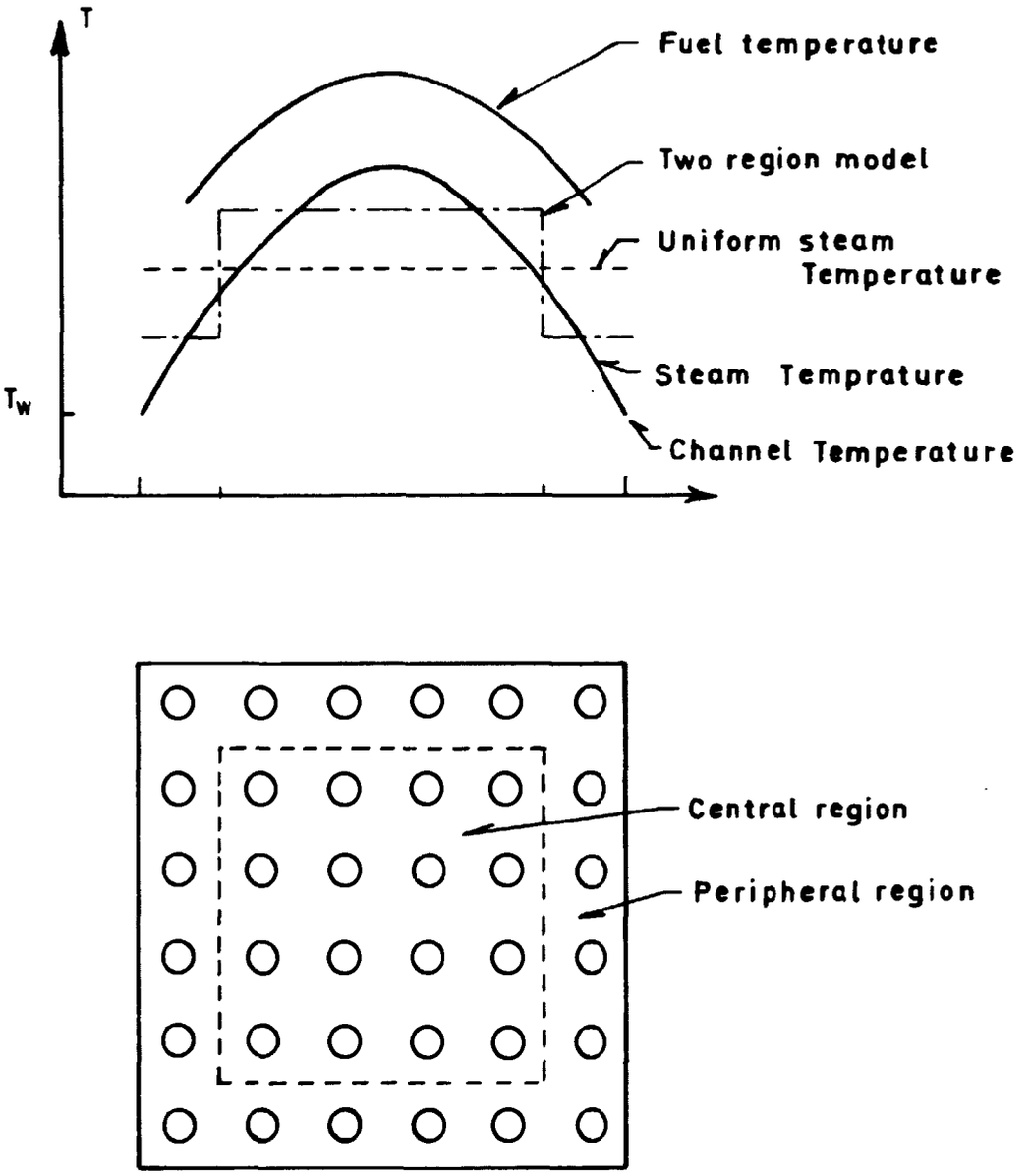

Fig.3.14. Two Region Steam Temperature Model

Because of the high steam superheat the temperature distribution can be found from the perfect gas law.

From conservation of mass we have

$$A_c \rho_c + A_p \rho_p = A_t \langle \rho \rangle \tag{3.83}$$

and from conservation of energy we have

$$A_c \rho_c T_c + A_p \rho_p T_p = A_t \langle \rho \rangle \overline{T} \tag{3.84}$$

For a perfect gas the equation of state is given by

$$\frac{P}{\rho} = kT \tag{3.85}$$

Combining (3.84) and (3.85) reduces (3.84) to an identity.

The assumption of a linear temperature drop to channel temperature gives

$$T_p = \tfrac{1}{2}(T_c + T_w) \tag{3.86}$$

Combination of (3.83), (3.85) and (3.86) gives

$$T_c = \frac{2A_p + A_c}{2A_t} \langle T \rangle - \tfrac{1}{2} T_w + \left\{ \left(\frac{2A_p + A_c}{2A_t} \langle T \rangle - \tfrac{1}{2} T_w \right)^2 + \langle T \rangle \, T_w \frac{A_c}{A_t} \right\}^{\frac{1}{2}} \tag{3.87}$$

and T_p is found from (3.84).

The two different steam temperatures are used in the calculation of the local convection heat transfer as well as the radiation heat transfer for the rods and the channel in the two regions.

3.6. The Equation of State

The equation of state of steam and water is represented as a set of polynomial approximations[24] to the VDI steam tables[25].

4. EXAMPLES ON CORECOOL CALCULATIONS

In order to demonstrate the applicability of CORECOOL a calculation for a typical ECCS experiment has been made. The calculation demonstrates the accuracy of CORECOOL, and it shows the amount of information which can be obtained from a CORECOOL-calculation.

The experiment is an ECCS experiment made in April 1974 by General Electric at their test facility[15] in San Jose.

The test facility is a full length fuel element with electrical heated stainless steel rods. The main data for the experiment are given in table 4.1.

Initial power, kW	250
Axial power peaking	1.3
Radial power peaking	1.14
Fuel rod length, m	3.76
Fuel rod diameter, m	$1.252 \cdot 10^{-2}$
Fuel rod pitch, m	$1.626 \cdot 10^{-2}$
Flow area in the element, m^2	$1.001 \cdot 10^{-2}$
Spray flow in fuel element, kg/s	0.156
Spray flow to by pass channel, kg/s	0.0313
Spray water temperature, ^{o}C	39
Pressure, bar	1.0
Maximum initial rod temperature, ^{o}C	760

Table 4.1. Data for the GE-ECCS experiment.

In fig. 4.1. is shown a comparison between the calculated maximum temperature in the fuel element and the measured maximum temperature, and it is seen that the difference is about 25^{o}C.

Fig. 4.2 shows the calculated temperatures vs. time. The rods were combined to 9 groups in the calculation. Group 1 is the water rod. The groups 2, 3 and 4 are central rods, group 8 the side rods, group 9 the corner rods and group 10 is the channel.

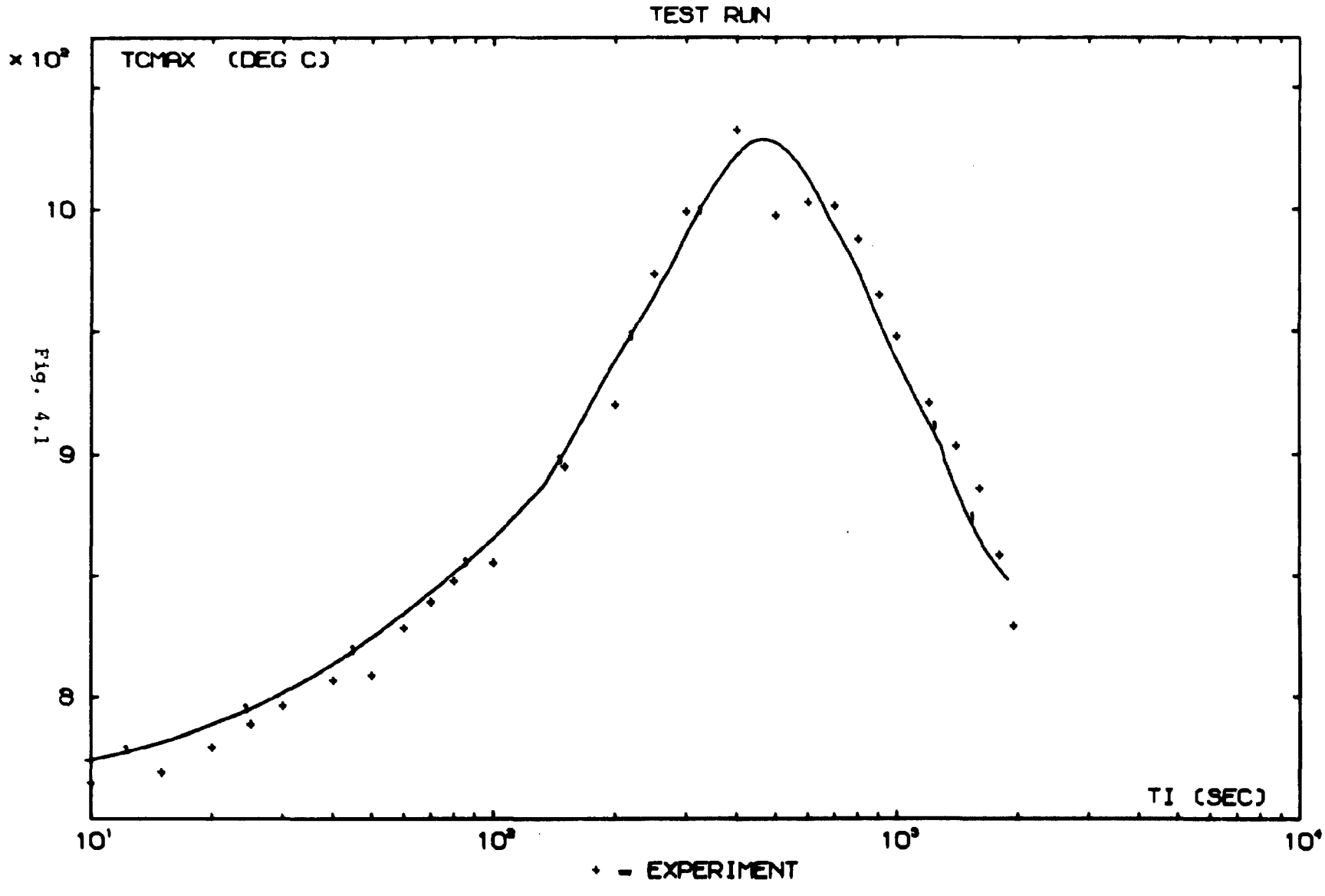
TEST RUN
TCMAX (DEG C)
x 10³
10
9
8
TI (SEC)
10¹
10²
10³
10⁴
+ - EXPERIMENT

Fig. 4.1

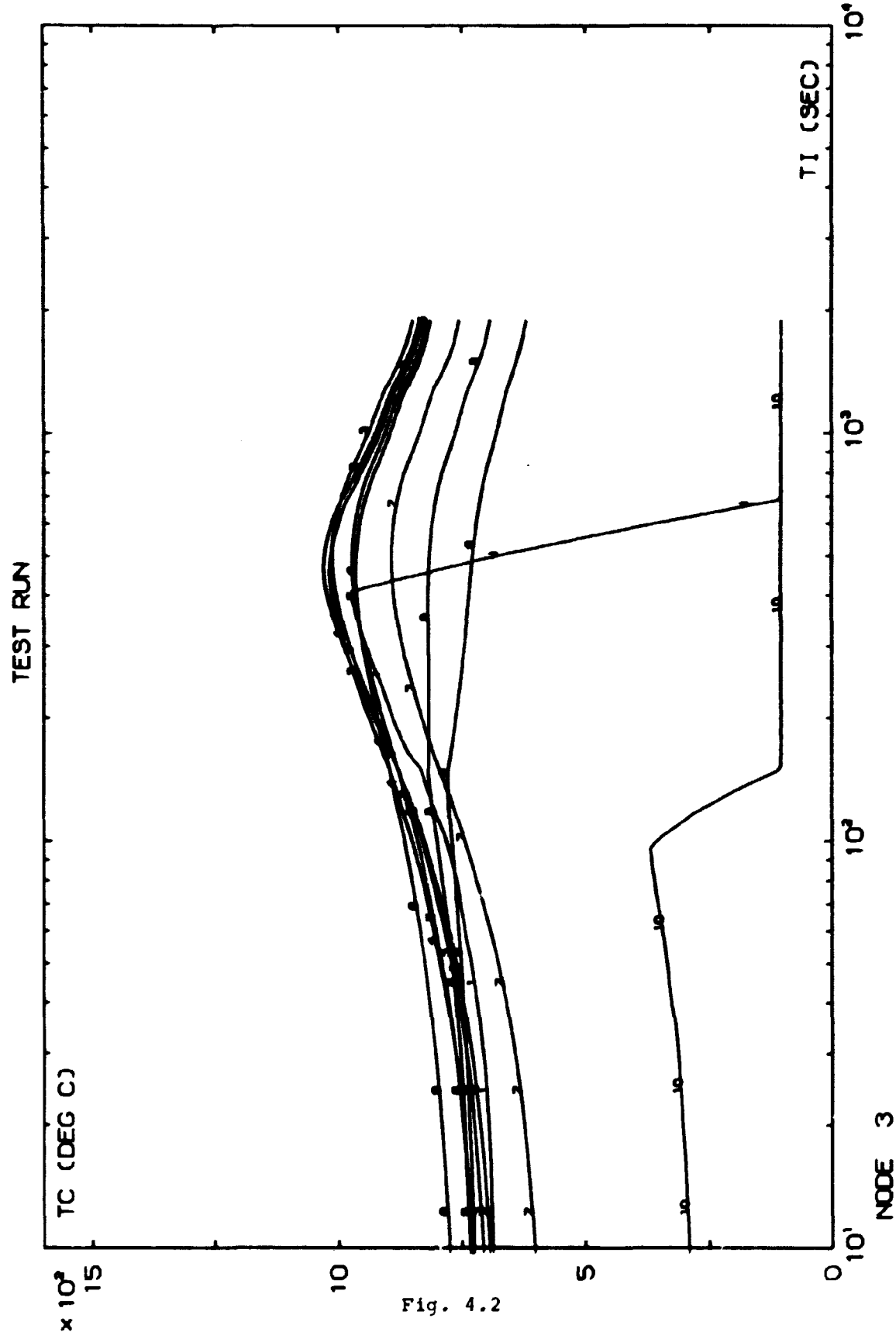

Fig. 4.2

As CORECOOL calculates the ECCS-transient for the whole fuel element, the temperatures, not only for the peak power level, but for whole fuel element are known. In fig. 4.3 and 4.4 are shown the calculated axial temperature-profiles for the center rods and the corner rods. The temperature profiles are shown for 0, 200, 400, 600 etc seconds after the start of the experiments, and the propagation of the rewetting fronts are noted at the top of the rods.

The calculation also allows an analysis of the energy generation and heat transfer in the fuel element. In table 4.2 is for the peak power level shown an energy balance for the fuel element to the times 0, 50, 100 and 450 sec. 50 sec is the time just before the rewetting front at the channel passes the peak power level and 100 sec is the time, when the rewetting front has passed. 450 sec is the time of the peak temperature. Around the sputtering front at the channel the droplet concentration and the evaporation are large, and the heat transfer to the two-phase flow will be large.

For the center rods and the corner rods the energy balance as function of the time is shown in fig. 4.5 and 4.6. Here

Time sec	0	50	100	450
Decay heat, kW/m	86.4	72.8	66.6	49.1
Total heat transfer from rods	17.0	34.9	44.0	46.2
Radiation from rods, kW/m	14.7	21.4	28.0	30.7
Convection from rods, kW/m	2.3	13.5	16.0	15.5
Stored in rods, kW/m	69.4	37.9	22.6	2.9
Radiation to channel, kW/m	14.5	15.0	25.4	28.1
Convection to channel, kW/m	1.3	0.9	1.1	1.5
Radiation to 2Ø, kW/m	0.2	6.4	2.6	2.6
Convection to 2Ø, kW/m	1.0	12.6	14.9	14.0

Table 4.2. Energy balance for the fuel element.

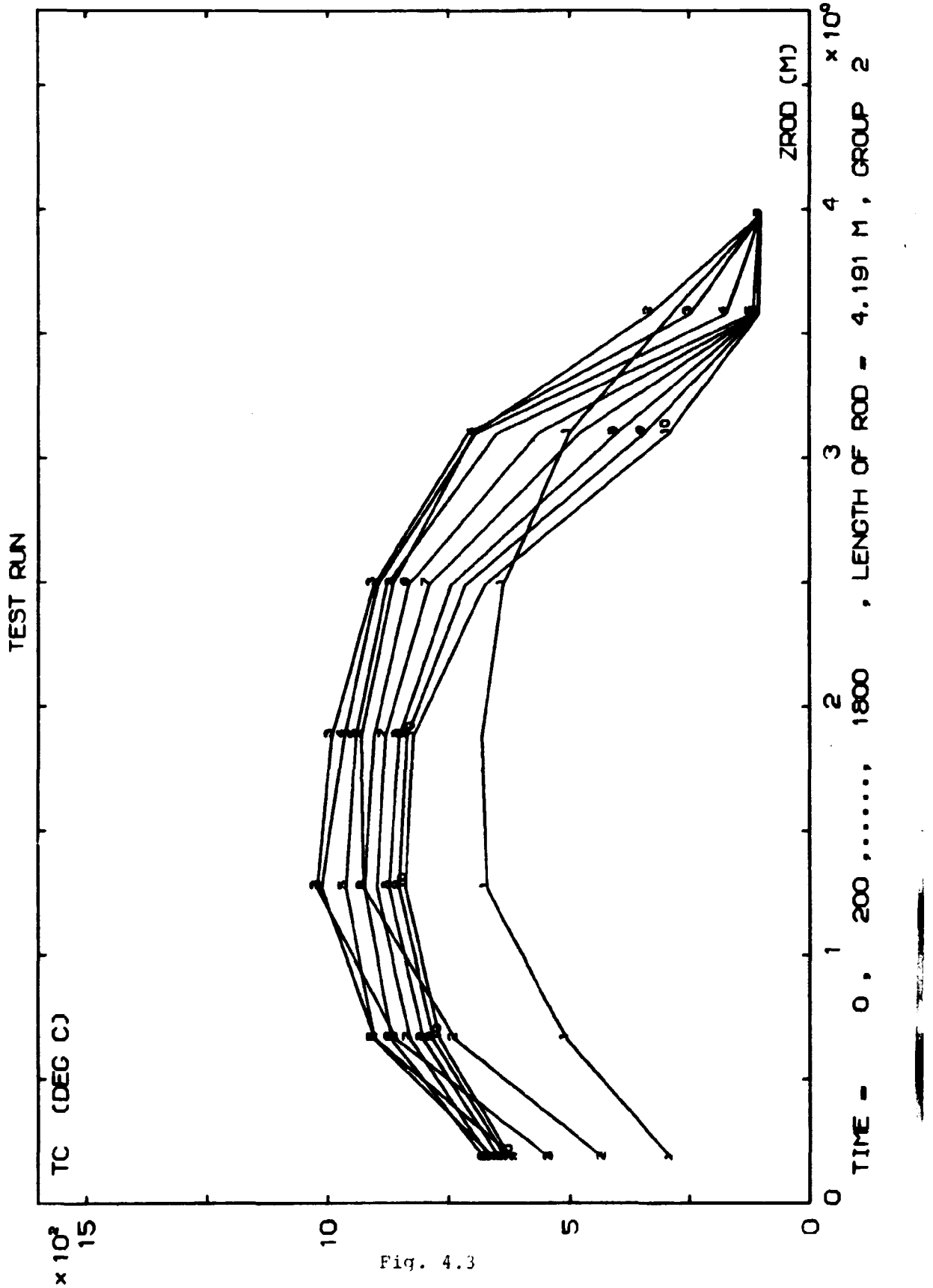
TEST RUN
TC (DEG C)
ZROD (M)
TIME = 0, 200 ,.....,
1800 , LENGTH OF ROD = 4.191 M , GROUP 2
x 10³
x 10⁰

Fig. 4.3

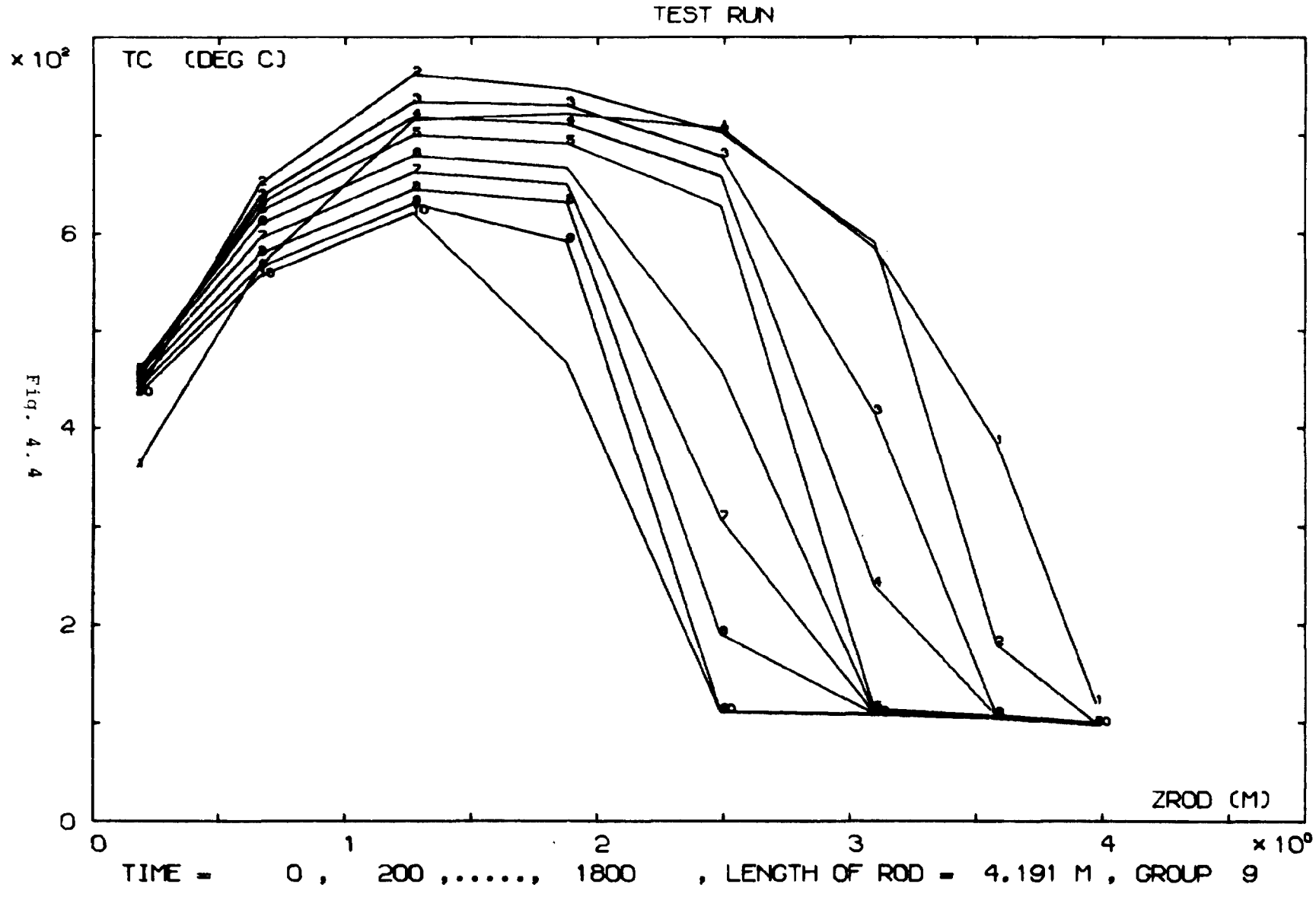
TEST RUN
TC (DEG C)
x 10²
6
4
2
0
0
1
2
3
4
x 10⁰
ZROD (M)
TIME = 0 , 200 ,....., 1800 , LENGTH OF ROD = 4.191 M , GROUP 9

Fig. 4.4

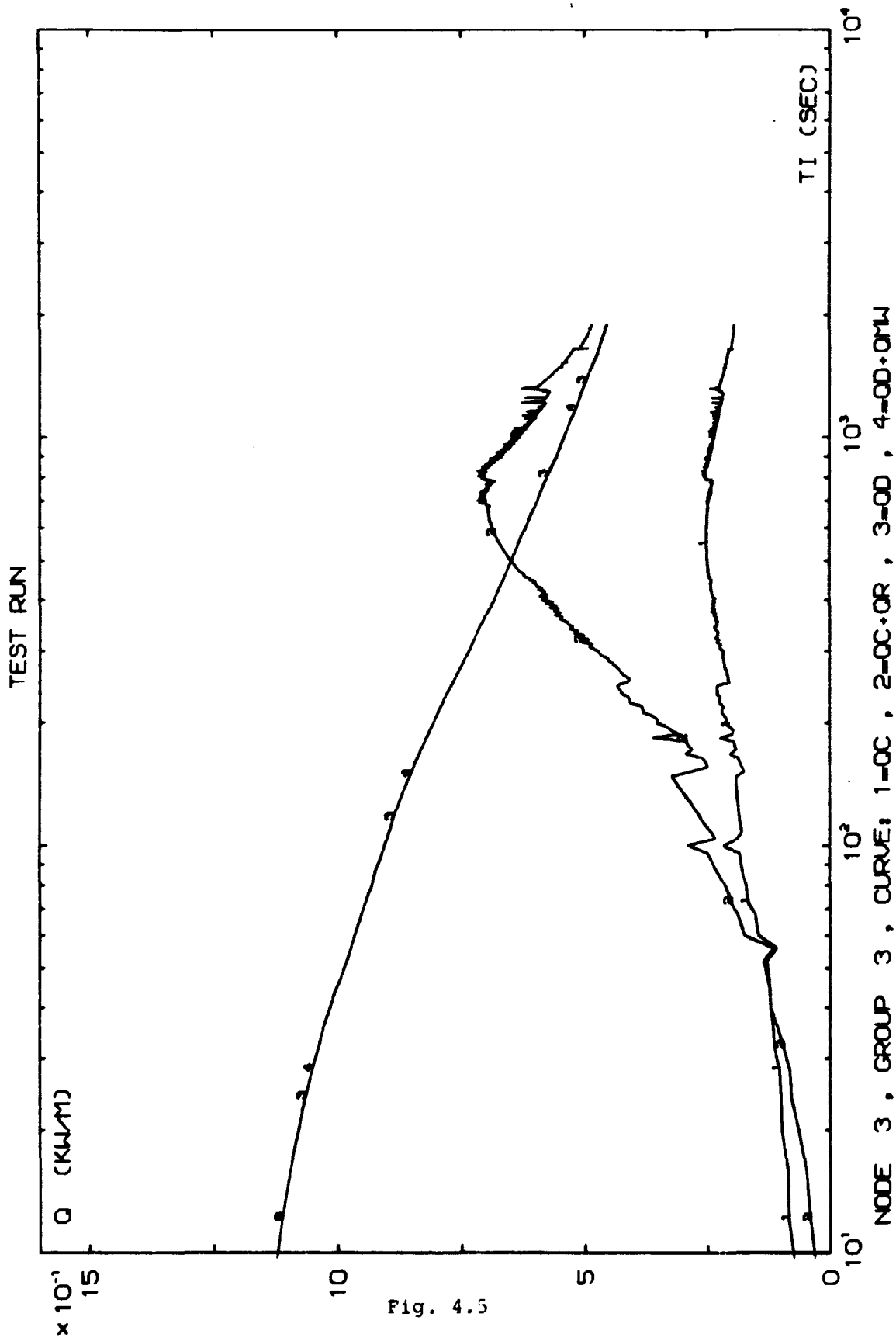
TEST RUN
Q (KW/M)
x 10⁻¹
15
10
5
0
10¹
10²
10³
10⁴
TI (SEC)
NODE 3 , GROUP 3 , CURVE: 1=QC , 2=QC+QR , 3=QD , 4=QD+QMW

Fig. 4.5

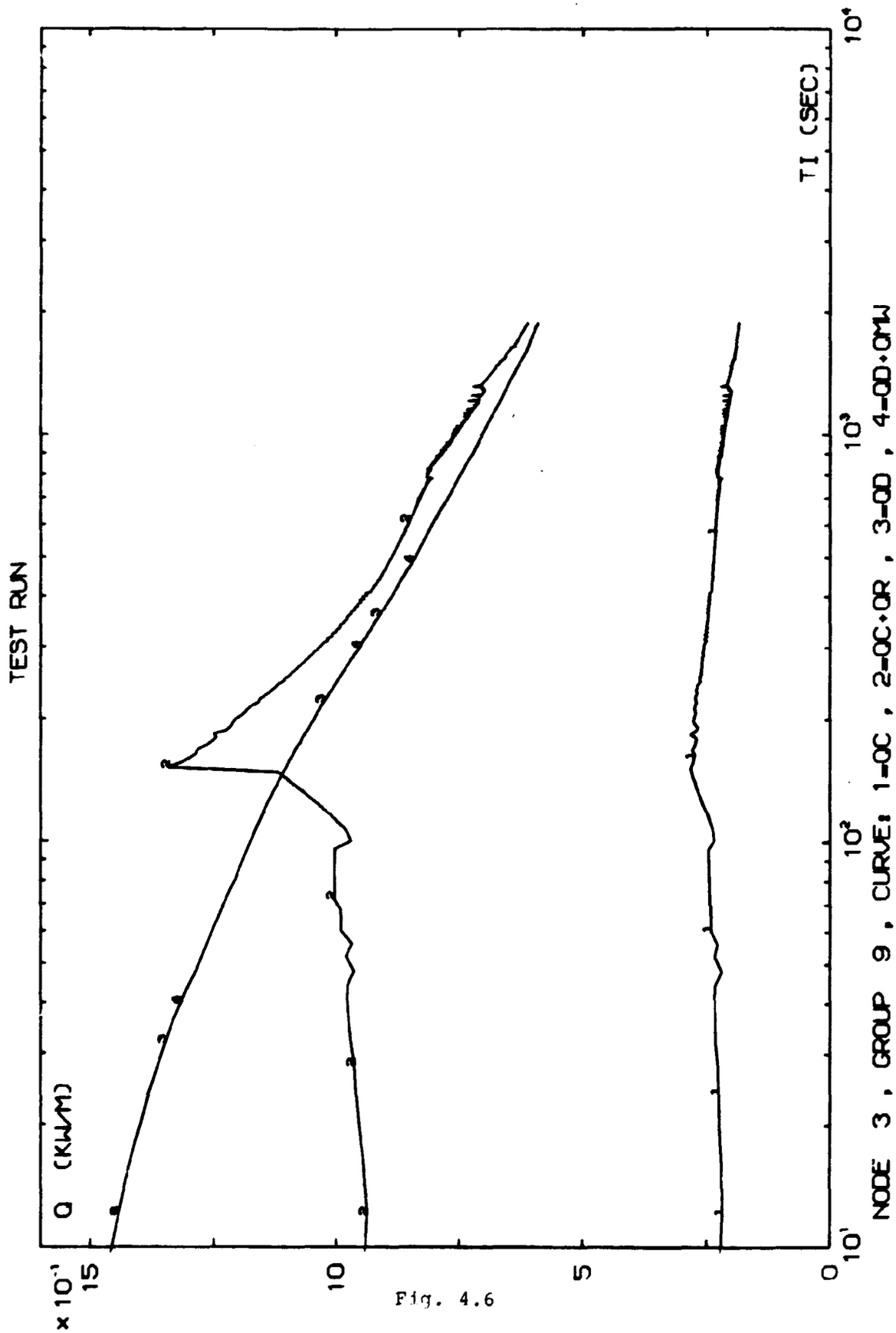
TEST RUN
Q (KW/M)
TI (SEC)
NODE 3 , GROUP 9 , CURVE: 1=QC , 2=QC+QR , 3=QD , 4=QD+QMW
x 10⁻¹
15
10
5
0
10¹
10²
10³
10⁴

Fig. 4.6

QC is the convection heat transfer
QR is the radiation heat transfer
QD is the decay heat
QMW is the energy production from the metal-water reaction.

As the two-phase flow in the fuel element is counter current the possibility of CCFL phenomena and flow oscillations exist. This did not happen in this run, but in fig. 4.7 is shown a typical case of flow oscillations in the bundle. The figure shows the steam and droplet velocities at the top of the fuel element.

VG is the steam velocity
VS is the droplet velocity.

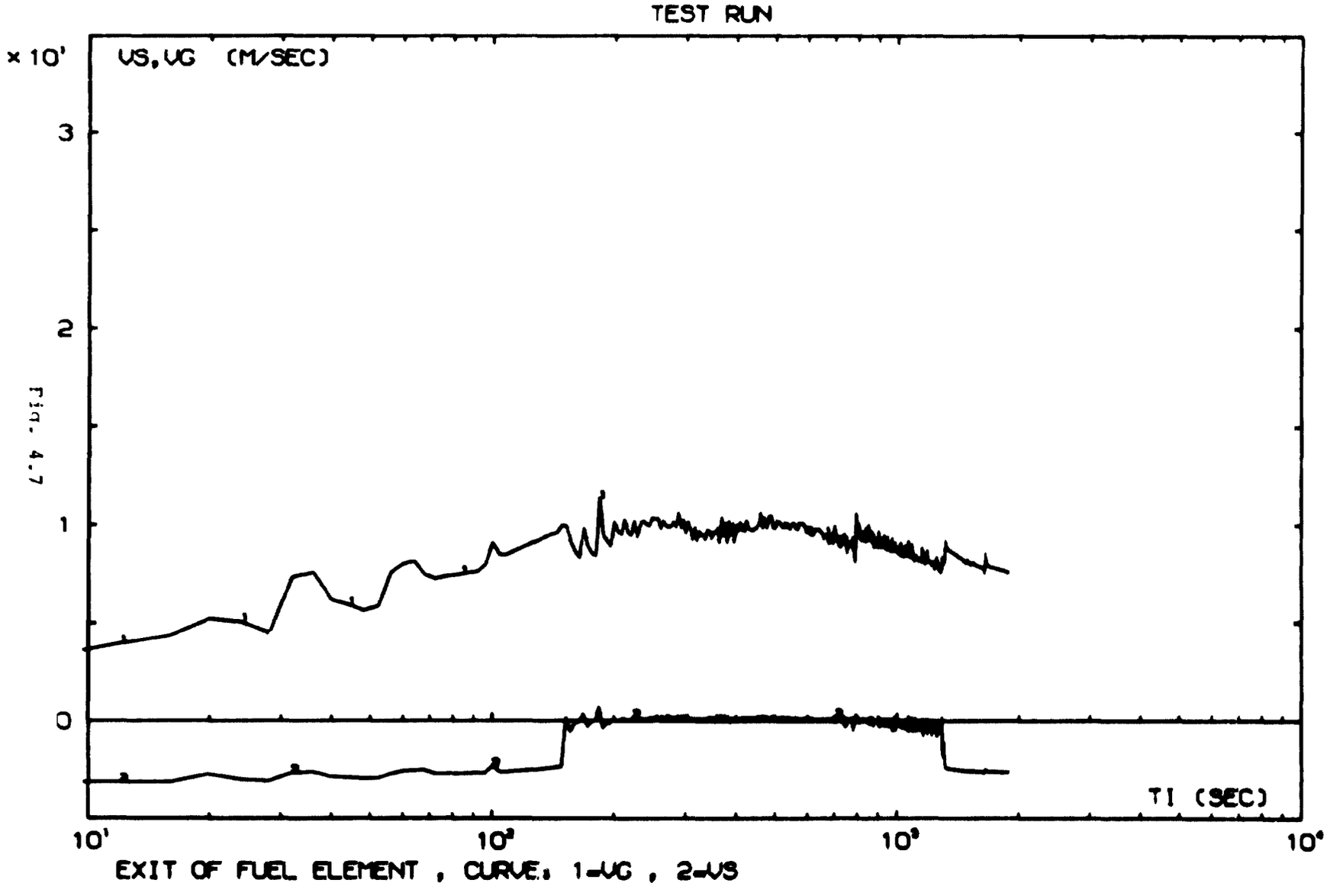
TEST RUN
× 10'
VS, VG (M/SEC)
3
2
1
0
TI (SEC)
10'
10²
10³
10⁴
EXIT OF FUEL ELEMENT , CURVE: 1-VG , 2-VS

Fig. 4.7

5. DISCUSSION AND CONCLUSION

CORECOOL, a model for emergency core spray cooling has been developed. The approach is not to use gross system dependent empirical correlations, but to base the model on an understanding of the different physical and chemical phenomena prevailing during a core heat-up transient, a detailed expression of these and the combination of these expressions, the conservation equations for the two-phase flow and the fuel rod model to the computer programme CORECOOL.

This approach has proven quite successful, not only is CORECOOL able to predict the overall behaviour of a fuel element during a core heat up transient but also many of the individual phenomena, such as rewetting, CCFL etc, occuring in the system. As the model is based on a modelling of the relevant individual phenomena, CORECOOL is not system dependent and is very well suited for parametric studies for both test facilities and nuclear power reactors. Furthermore conservatism, caused by lack of sophistication, in the present models can be abandonned thus reducing the calculated peak cladding temperature.

However, some improvemen and further development of the model are needed. A better understanding of the CCFL phenomenon and the importance of the droplet distribution is desirable, and the inclusion of a fuel rod failure model is needed.

In connection with bottom flooding the model is still applicable, but should be used only for the part of the system above the two-phase level. Accordingly the development of a model able to trace the liquid inventory in the system and the swell of the two-phase level is needed.

6. ACKNOWLEDGEMENT

The authors gratefully acknowledge the assistance, many helpful suggestions and comments of Drs. Gary E. Dix, Jose M. Gonzalez*), and K.H. Sun of General Electric Company, professor C.L. Tien of University of California, Berkeley, Department of Mechanical Engineering, and A. Olsen of Risø National Laboratory.

*) Now the Free University of Azcapotzalco, Mexico.

7. REFERENCES

1) J.G.M. Andersen, REMI/HEATCOOL, A Model for Evaluation of Core Heat-Up and Emergency Core Cooling System Performance for Light-Water Cooled Nuclear Power Reactors. RR 296, Danish AEC (1973) 86 pp.

2) G.B. Wallis, One-dimensional Two-phase Flow (McGraw-Hill, New York, 1969) 408 pp.

3) R.S. Brodkey, The Phenomena of Fluid Motions. (Addison-Wesley, Reading, Mass., 1967) 737 pp.

4) Lord S. Rayleigh, On the Instability of Jets. Proc. Lond. Math. Soc. 10 (1878/79) 4-13.

5) A.C. Merrington and E.G. Richardson, The Break-Up of Liquid Jets. Proc. Phys. Sec. (London) 59 (1947) 1-13.

6) D.J. Hanson et al. ECC Performance in the Semiscale Geometry. ANCR-1161, June 1974.

7) Proposed ANS Standard, Decay Energy Release Rates following Shutdown of Uranium-fueled Thermal Reactors, Approved by Subcommittee. ANS-5.1 (1971) 7 pp.

8) L. Baker and L.C. Just, Studies of Metal-Water Reactions at High Temperatures. ANL-6548 (1962) 86 pp.

9) United States Atomic Energy Commission, 10 CFR 50, Appendix K, January 1974.

10) P.N. Rowe, K.T. Claxton, and J.B. Lewis, Heat and Mass Transfer from a Single Sphere in an Extensive Flowing Fluid. Trans. Inst. Chem. Eng. 43 (1965) T14-T31.

11) J.C. Hesson, J.L. Anderson, and R.O. Ivins, CHEMLOC-II: A Computer Program Describing the Core Heating and Cladding - Steam Reaction for a Water-Cooled Power Reactor following a Loss of Coolant. ANL-7361 (1968) 115 pp.

12) F.W. Dittus and L.M.K. Boelter, Univ. Calif., Pubs. Eng., 2, 443 (1930).

13) K.H. Sun, J.M. Gonzalez and C.L. Tien, Calculation of Combined Radiation and Convection Heat Transfer in Rod Bundles Under Emergency Cooling Conditions, ASME-paper, (August 1975).

14) J.D. Duncan and J.E. Leonard, BWR Standby Cooling Heat Transfer Performance under Simulated Loss-of-Coolant Conditions between 15 and 300 psia. GEAP-13190 (1971) 220 pp.

15) J.D. Duncan and J.E. Leonard, Emergency Cooling in Boiling Water Reactors under Simulated Loss-of-Coolant Conditions. BWR-FLECHT Final Report. GEAP-13197 (1971) 86 pp.

16) J.G.M. Andersen and P. Hansen, Two-Dimensional Heat Conduction in Rewetting Phenomena, NORHAV-D-6, Danish AEC, (1974).

17) C.L. Tien and L.S. Yao, Analysis of Conduction Controlled Rewetting of a Vertical Surface, ASME paper (November 1974).

18) M.W.E. Coney, Calculations on the Rewetting of Hot Surfaces, Nucl. eng. des. (1974) 246-259.

19) A.W. Bennet et al., The Wetting of Hot Surfaces by Water in a Steam Invironment at High Pressure, AERE-R5146, 1966.

20) R.B. Duffey, and D.T.C. Porthouse, "Experiments on the Cooling of High-Temperature Surfaces by Water Jets and Drops", Report No. RD/B/N2386, Berkeley Nuclear Laboratories, England, August 1972.

21) L.S. Tong, Boiling Heat Transfer and Two-Phase Flow (Wiley, New York, 1965) 242 pp.

22) J.G.M. Andersen, A radiation Model with Transport Correction, to be published.

23) M.M. Abu-Romia and C.L. Tien, Appropriate Mean Absorption Coefficients for Infrared Radiation of Gases, J. Heat Transfer, 89C, 321-327 (1967).

24) M. Hjelm-Hansen, Polynomial Approximations of Thermodynamic Properties of Light Water, Risø-M-669, (1967) 32 pp.

25) E. Smidt (editor), Properties of Water and Steam in SI-Units, kJ, bar, 0-800°C, 0-1000 bar. (Springer, Berlin, 1969) 205 pp.

26) E.M. Sparrow and R.D. Cess, Radiation Heat Transfer (Brooks/Cole, Belmont, Calif., 1970) 340 pp.

8. NOMENCLATURE

Name	Unit	Content
A	m^2	Cross section
a	m^{-1}	Absorption coefficient
a	s/m^2	Auxilary constant, $\frac{\rho c}{k}$
B	W/m^2	Radiosity
B	kg/m^2s^2	Momentum source
b	kg/m^2s^2	Interfacial shear
Bi	-	Biot number
C	-	Constant in CCFL correlation
C	-	Loss coefficient
c	-	Correction factor in momentum equation
c	J/kg	Heat capacity
D	m	Diameter
d	m	Diameter
ΔE	J/mole	Activation energy
F	-	View factor
f	kg/ms^2	Friction
f	-	Auxilary function
G	kg/m^2s	Specific mass flow (3.5)
G	kg/ms	Specific mass flow for films
g	m/s^2	Acceleration of gravity
H	W/m^2	Incident radiation
h	J/kg	Enthalpy
h	$W/m^2\ ^oC$	Heat transfer coefficient
I	kg/ms	Integrated momentum
I	-	Modified Bessel function of 1. art
I	W/m^2	Radiation flux
j	m/s	Volumetric flux
j^*	-	Dimensionless flux
K	m^2/s	Constant for metal-water reactions
K	-	Kutateladze number
k	$W/m\ ^oC$	Thermal conductivity
k	m^{-1}	Wave number
L	m	Length
M	kg	Mass
m	kg	Mass
$\dot{m}$	kg/m^3s	Change of mass

Name	Unit	Content
N	-	Number
n	m^{-3}	Number density
n	-	Number
$\dot{n}$	$m^{-3}\ s^{-1}$	Change of number density
Nu	-	Nusselt number
P	N/m^2	Pressure
p	m	Pitch
Pe	-	Peclet number
Pr	-	Prandtl number
Q'''	W/m^3	Energy generation
q"	W/m^2	Energy flux
q'''	W/m^3	Energy generation
Q_M	J/kg	Energy production.
R	J/mole ^oC	Gas constant
R	m^{-2}	Resistance in electrical analog
r	m	Radius
Re	-	Reynolds number
S	m	Perimeter
S	W/m^2	Black body radiation
s	m	Thickness
T	^oC, ^oK	Temperature
t	s	Time
u	m/s	Velocity
V	m^3	Volume
W	kg/s	Mass flow
We	-	Weber number
x	-	Auxilary variable
t	m	Length

GREEK LETTER

Name	Unit	Content
α	-	Void fraction
α	-	Deformation of droplet
β	$W/m^3\ ^oC$	Heat transfer coefficient
ε	-	Emissivity
λ	m	Wave length
μ	-	Anisotropic reflection
ϕ	$kg/m^3\ s$	Evaporation/condensation
ϕ	rad	Angle
Ω	m^3/s	Volume flow
θ	-	Dimensionless temperature
θ	rad	Inclination
ρ	kg/m^3	Density
σ	N/m	Surface tension
σ	$W/m^2\ ^oK^4$	Stefan Blotzmanns constant
ω	s^{-1}	Frequency
τ	-	Transmissivity
τ	s	Time constant
ν	m^3/kg	Specific volume

SUBSCRIPTS

Name	Content
c	Central
ci	Core inlet
D	Drag
d	Droplet
F	Friction
f	Film
fr	Front
g	Steam
gℓ	Steam to steam-water interface
h	Hydraulic
i	Indices
j	Indices
L	Loss
ℓ	Water
s	Saturation
s	Surface
sg	Saturated steam
t	Total
w	Wall

Superscripts

n	Time step

APPENDIX A

Jet and Droplet instability

A liquid jet is basically unstable, a small perturbation on the surface will grow, and finally cause the disintegration of the jet.

Let us consider a sinousodial perturbation as shown in fig. A.1. The cross section of the jet is given by

$$A(x) = A_o(1 + a\cos(kx)) \tag{A.1}$$

and for small perturbation, i.e. $a << 1$, the radius is given by

$$r(x) = r_j(1 + \frac{a}{2}\cos(kx)) \tag{A.2}$$

The pressure in the liquid is given by

$$P(x) = P_s(x) + P_g(x) \tag{A.3}$$

where

P_s is the pressure contribution from the surface tension,

and P_g is the pressure arising from the velocity distribution in the gas.

The first one is given by

$$P_s(x) = \sigma(\frac{1}{r(x)} + \frac{\partial^2 r}{\partial x^2}) = \frac{\sigma}{r_j}(1 - \frac{a}{2}(1-(kr_j)^2)\cos(kx)) \tag{A.4}$$

Assuming potential flow for the gas the first order approximation to the velocity distribution relative to the jet is

$$U_{gx} = U_o(1 + \frac{a}{2} kr_j \frac{r_j}{r} e^{-k(r-r_j)}\cos(kx)) \tag{A.5}$$

$$U_{gy} = -U_o \frac{a}{2} kr_j \frac{r_j}{r} e^{-k(r-r_j)}\sin(kx) \tag{A.6}$$

For potential flow the pressure is given by

$$\nabla P_g = -\rho_g \bar{u}\cdot\nabla\bar{u} \tag{A.7}$$

and for $r=r_o$ we get

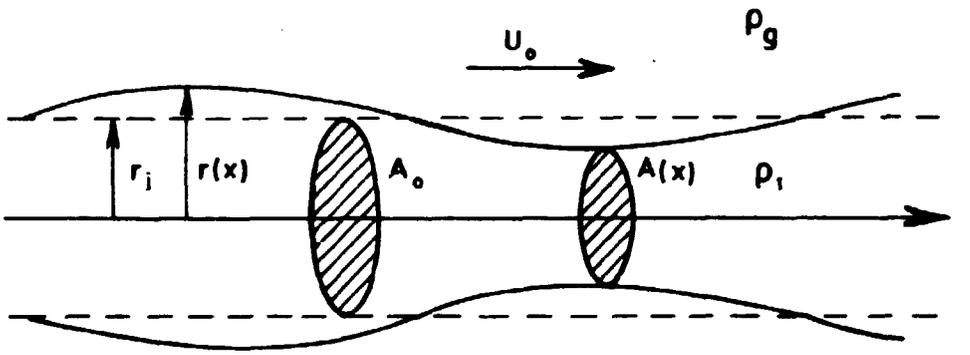

Fig. A.1. Liquid jet with a sinousodial perturbation.

$$\frac{\partial P_g}{\partial x} = \tfrac{1}{2}\,\rho_g\,U_o^2\,a\,k^2\,r_j\,\sin(kx) \tag{A.8}$$

A first order approximation to the continuity and momentum equation for the liquid is given by

$$\frac{\partial A}{\partial t} = -\frac{\partial}{\partial x}(A\,u_\ell) \tag{A.9}$$

$$\rho_\ell\,\frac{\partial u_\ell}{\partial t} = -\frac{\partial P}{\partial x} \tag{A.10}$$

Using (A.4) and (A.8) a solution to (A.9) and (A.10) can be found

$$a = a_o\,e^{\omega t} \tag{A.11}$$

$$U_\ell = -\frac{k\,a_o}{\rho_\ell\,\omega}\left(\frac{\sigma}{2r_j}(1-(kr_j)^2)+kr_j\,\rho_g\,U_o^2\right)\sin(kx)e^{\omega t} \tag{A.12}$$

where

$$\omega^2 = \frac{\sigma}{2\rho_\ell\,r_j^3}(kr_j)^2(1-(kr_j)^2 + \tfrac{1}{2}\,kr_j\,We_j) \tag{A.13}$$

$$We_j = \frac{2r_j\,\rho_g\,U_o^2}{\sigma} \tag{A.14}$$

From (A.13) it is seen that the jet is only unstable for

$$kr_j < \frac{We_j}{4} + \sqrt{\left(\frac{We_j}{4}\right)^2 + 1} \tag{A.15}$$

and that the maximum growth rate is obtained for

$$kr_\Phi = \frac{3}{16}\,We_j + \sqrt{\left(\frac{3}{16}\,We_j\right)^2 + \tfrac{1}{2}} \tag{A.16}$$

Assuming that the jet will break up at a wave-length corresponding to the maximum growth rate the diameter of the produced droplets will be given by

$$\frac{d_d}{2r_j} = \left\{\frac{3\pi}{\frac{3}{8}\,We_j + \sqrt{\left(\frac{3}{8}\,We_j\right)^2 + 2}}\right\}^{\frac{1}{3}} \tag{A.17}$$

and the length of the jet

$$L_j = r_j \ln\left(\frac{r_j}{\Delta r}\right)\sqrt{\frac{\rho_l}{\rho_g}}\,\frac{\sqrt{We_j}}{\left\{\frac{3}{16}We_j+\sqrt{\left(\frac{3}{16}We_j\right)^2+\frac{1}{2}}\right\}\left\{\frac{1}{2}+\frac{3}{128}We_j^2+\frac{1}{8}We_j\sqrt{\left(\frac{3}{16}We_j\right)^2+\frac{1}{2}}\right\}^{\frac{1}{2}}} \tag{A.18}$$

where Δr is the size of the initial perturbation.

In fig. A.2 is given a plot of (A.17) and in fig. A.3 a plot of (A.18).

The droplets produced by the jet may be unstable and break up into smaller droplets. Due to the gas flow around the droplet a pressure distribution as shown in fig. A.4 will exist

$$\Delta P_g = \tfrac{1}{2}\,\rho_g\,U_d^2 \tag{A.19}$$

This pressure distribution will deform the droplet until a balance with the surface tension is obtained. Assuming the droplet has the shape of an elipsoide with rotational symmetry the shape will be given by

$$\frac{x^2}{r_x^2} + r_x\,\frac{r^2}{r_d^3} = 1 \tag{A.20}$$

where r_x is half the thickness of the droplet in the direction of motion.

Defining $\alpha = \frac{r_x}{r_d}$ we get

$$\left(\frac{x}{\alpha}\right)^2 + \alpha r^2 = r_d^2 \tag{A.21}$$

As the pressure increment from the surface tension is given by

$$\Delta P_s = \sigma\left(\frac{1}{R_1} + \frac{1}{R_2}\right) \tag{A.22}$$

where R_1 and R_2 are the two radii of curvature, the pressure difference between the point $(o, \frac{r_d}{\sqrt{\alpha}})$ and $(\alpha r_d, o)$ can be evaluated to

$$\Delta P_s = \frac{\sigma}{r_d}\left(\alpha^{0.5} + \alpha^{-2.5} - 2\alpha^2\right) \tag{A.23}$$

For the droplet to be in equilibrium we must have

$$\Delta P_s = 2\Delta P_g \tag{A.24}$$

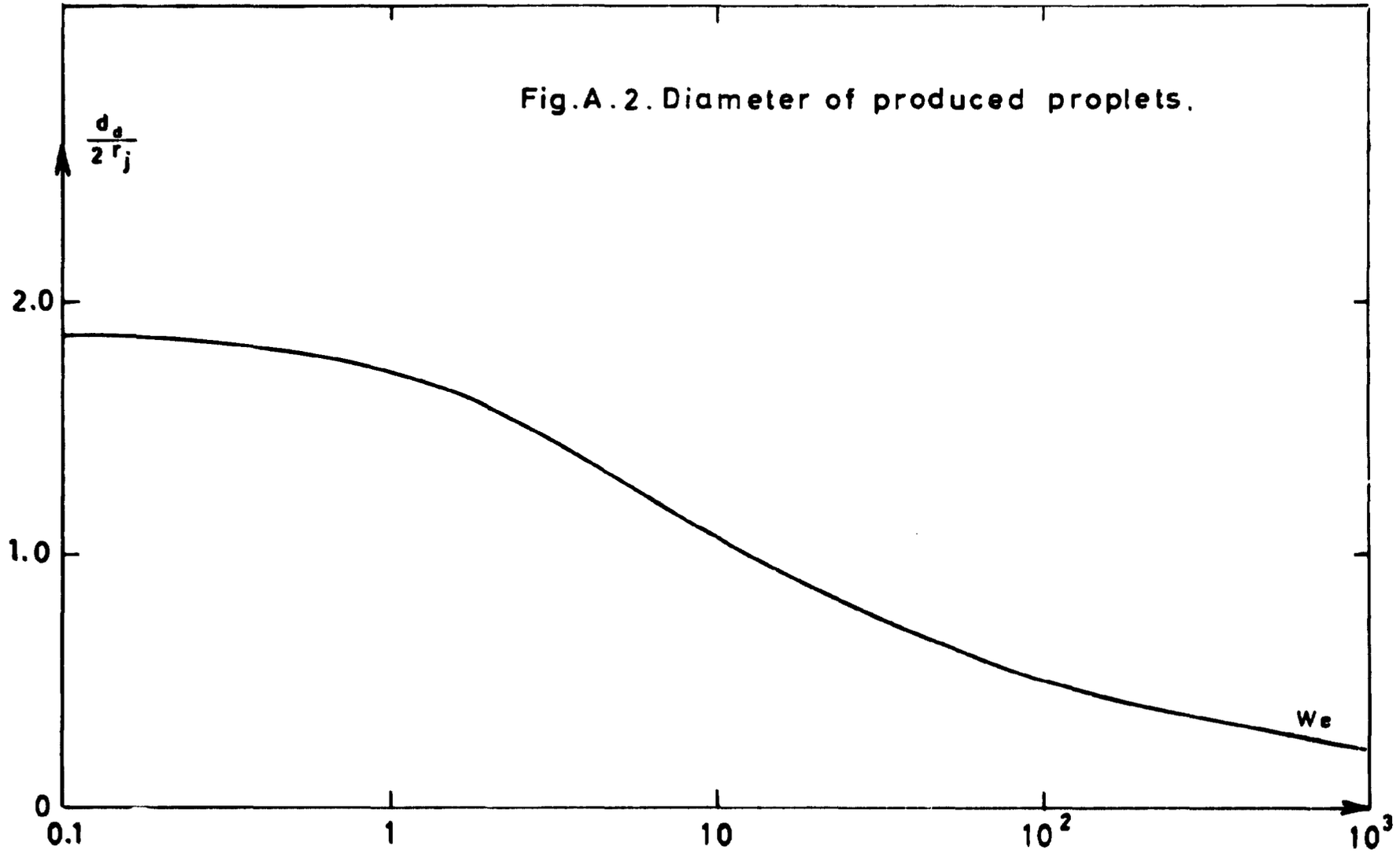

Fig.A.2. Diameter of produced proplets.

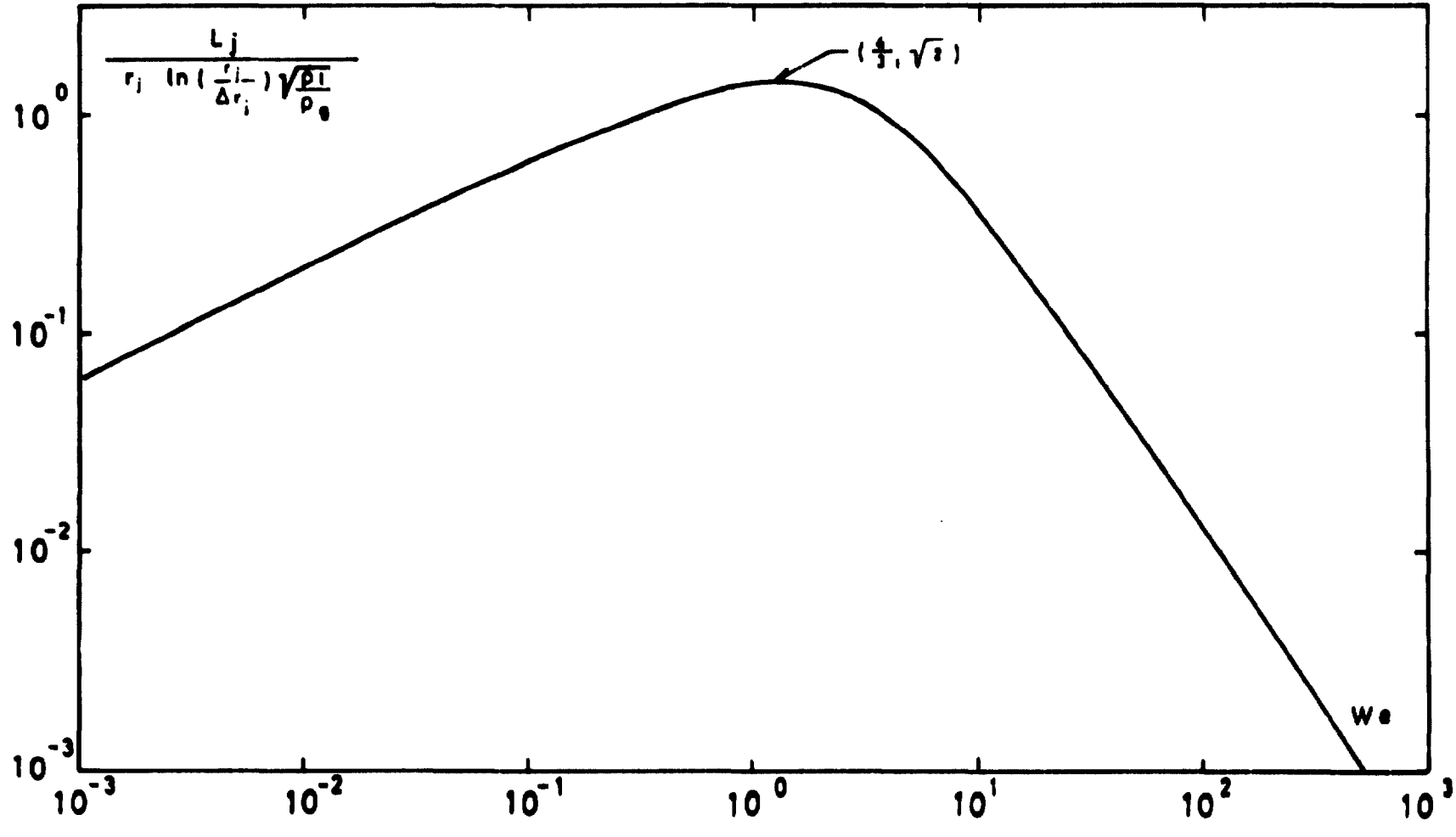

Fig. A.3. Length of jet as function of Weber number

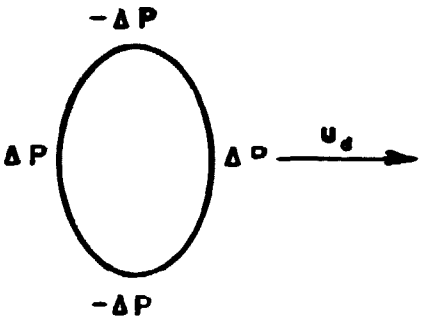

Fig. A.4. Pressure distribution around a droplet.

or

$$\alpha^{0.5} + \alpha^{-2.5} - 2\alpha^2 = \tfrac{1}{2}\, We_d \tag{A.25}$$

where

$$We_d = \frac{2r_d\, \rho_g\, u_d^2}{\sigma} \tag{A.26}$$

The surface area of the droplet is given by

$$A_d = 4\pi r_d^2 \left(\frac{1}{2\alpha} + \sqrt{\alpha}\, \frac{\ln(\alpha^{-1.5} + \sqrt{\alpha^{-3} - 1})}{2\sqrt{\alpha^{-3} - 1}}\right) \tag{A.27}$$

and if the droplet has to break up without additional work, the surface area has to be maintained. Assuming the daughter droplets to be spherical from conservation of volume and surface area the number of produced can easily be determined to

$$n = \left(\frac{1}{2\alpha} + \sqrt{\alpha}\, \frac{\ln(\alpha^{-1.5} + \sqrt{\alpha^{-3} - 1})}{2\sqrt{\alpha^{-3} - 1}}\right)^3 \tag{A.28}$$

The radius of the daughter droplets is

$$r = r_d\, n^{-\frac{1}{3}} \tag{A.29}$$

A plot of (A.25) and (A.27) is given in fig. A.5 and A.6.

A droplet can at least break up into two droplets and inserting $n = 2$ in equation A.28 gives

$$\alpha' = 0.48$$

and using this in equation A.25 gives the critical Weber number for droplet break up

$$We = 13.1\ .$$

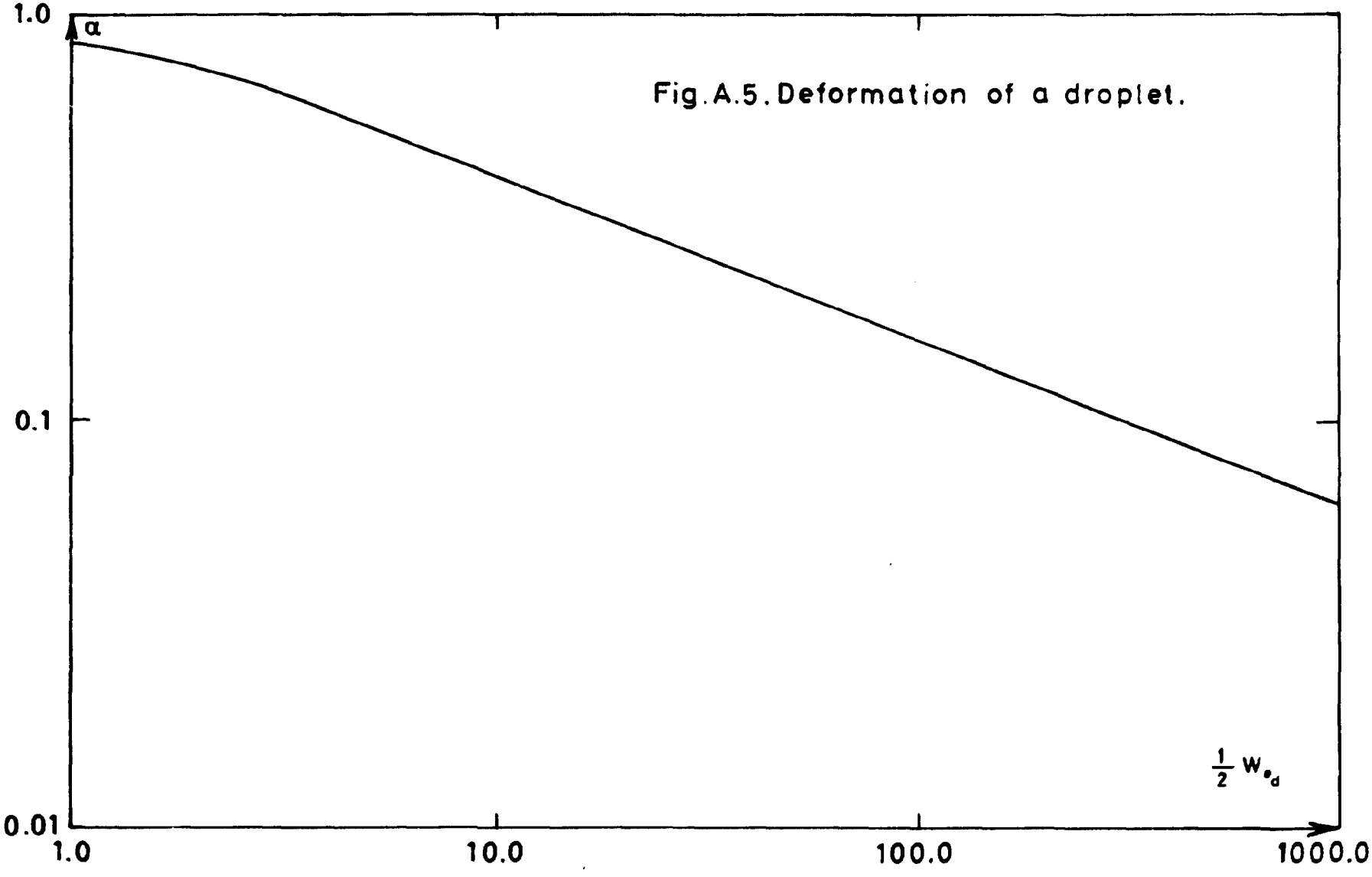

Fig. A.5. Deformation of a droplet.

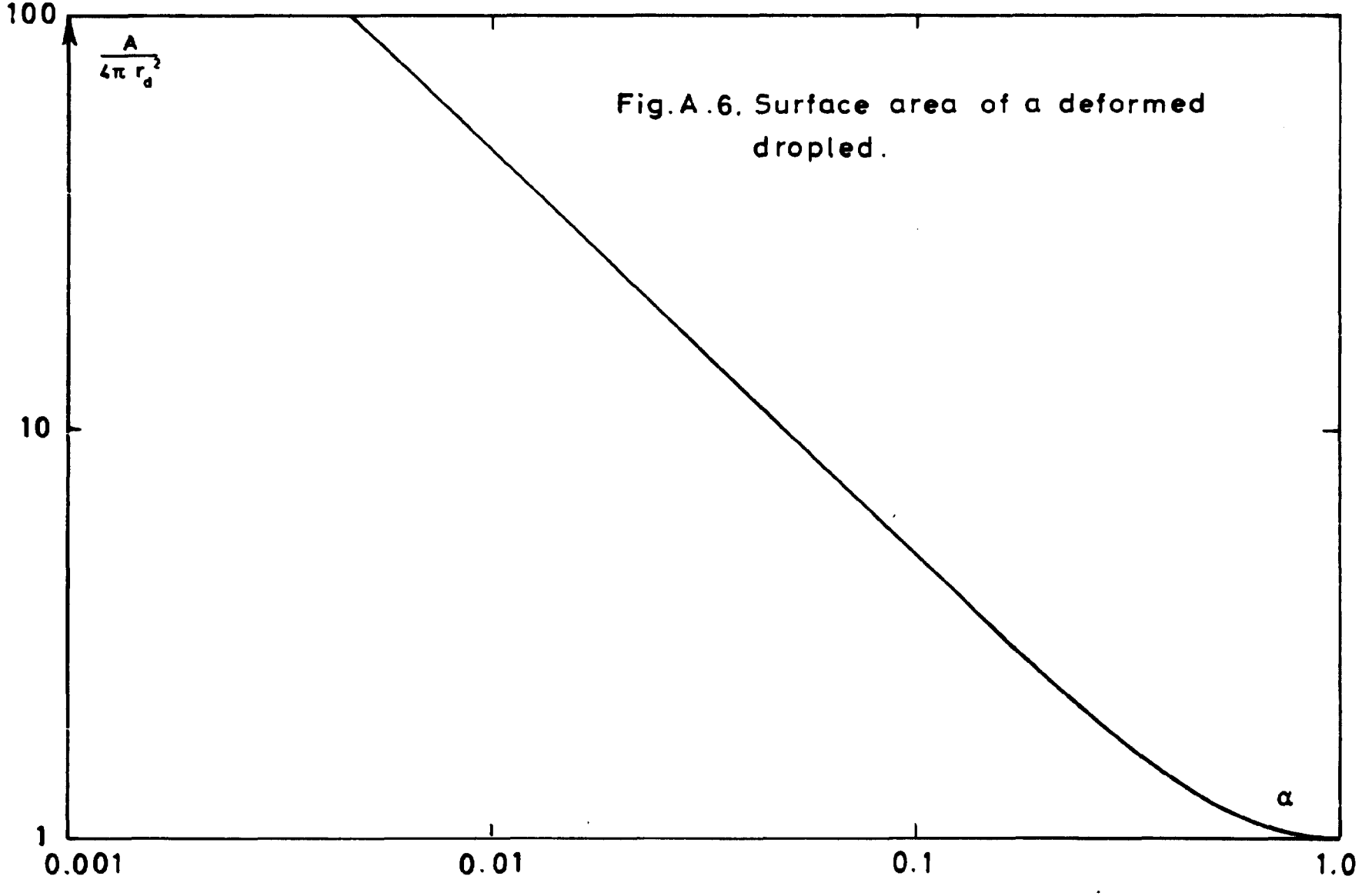

Fig. A.6. Surface area of a deformed dropled.

APPENDIX B

Heat Transfer in a Spherical Droplet

In accordance with section 2 it is assumed that the temperature at a steam-liquid interface will be the saturation temperature. A further assumption is, that, if a droplet with the temperature T_d is introduced in a steam atmosphere, the saturation temperature at the surface will immediately be established. This is the problem to be solved.

Subtracting T_d from all temperatures we have

$$\rho c \frac{\partial T}{\partial t} = k\left\{ \frac{\partial^2 T}{\partial r^2} + \frac{2}{r} \frac{\partial T}{\partial r} \right\} \tag{B.1}$$

and the boundary conditions

$$T(r,0) = 0 \qquad \text{for } 0 \leq r < r_o \tag{B.2}$$

$$T(r_o,t) = T_s \qquad \text{for } 0 \leq t < \infty \tag{B.3}$$

$$\frac{\partial T}{\partial r}\Big|_{r=0} = 0 \qquad \text{for } 0 \leq t < \infty \tag{B.4}$$

Introducing

$$a = \frac{\rho c}{k} \tag{B.5}$$

$$f(r,s) = \hat{L}\, T(r,t) \tag{B.6}$$

where $\hat{L}$ indicates the Laplace transformation, we obtain using (B.1) and (B.2)

$$\frac{\partial^2 f}{\partial r^2} + \frac{2}{r} \frac{\partial f}{\partial r} - asf = 0 \tag{B.7}$$

which has the solution

$$f(r,s) = \frac{1}{r} \left\{ C_1(s) e^{-r\sqrt{as}} + C_2(s) e^{r\sqrt{as}} \right\} \tag{B.8}$$

where C_1 and C_2 are arbitrary functions in s.

Using the conditions (B.3) and (B.4) we obtain

$$f(r,s) = \frac{r_o T_s' \sinh(r\sqrt{as})}{r\, s \sinh(r_o\sqrt{as})} \tag{B.9}$$

(B.9) has the poles

$$s_n = -\frac{1}{a}\left(\frac{\pi}{r_o} n\right)^2 , \qquad n = 0, 1, 2, ... \tag{B.10}$$

and the residua

$$res_n = \begin{cases} T_s' & \text{for } n = 0 \\ T_s' \dfrac{2r_o \sin(\frac{r}{r_o} n\pi)}{rn\pi(-1)^n} & \text{for } n = 1, 2, 3, ... \end{cases} \tag{B.11}$$

Using Heaviside's expansion theorem we obtain

$$T(r,t) = T_s' \left\{1 + \frac{r_o}{r} \sum_{n=1}^{\infty} \left(\frac{2\sin(\frac{r}{r_o} n\pi)}{n\pi(-1)^n} e^{-\frac{1}{a}\left(\frac{\pi}{r_o} n\right)^2 t}\right)\right\} , \tag{B.12}$$

and it can easily be shown that the boundary conditions (B.2), (B.3), and (B.4) are fulfilled. Consequently (B.12) represents the correct solution to the problem.

The heat transfer Q(t) to the surface is given by

$$Q(t) = 4\pi r_o^2 k \left.\frac{\partial T}{\partial r}\right|_{r=r_o} = 8\pi r_o k T_s' \sum_{n=1}^{\infty} e^{-\frac{1}{a}\left(\frac{\pi}{r_o} n\right)^2 t} \tag{B.13}$$

For $t << a\left(\frac{r_o}{\pi}\right)^2$ (B.13) becomes

$$Q(t) \approx 4r_o^2 k T_s' \sqrt{\frac{a\pi}{t}} = 4\pi\, r_o k T_s' \sqrt{a\left(\frac{r_o}{\pi}\right)^2 \frac{\pi}{t}} \tag{B.14}$$

and for $t > a\left(\frac{r_o}{\pi}\right)^2$ only the first term in the sum is important, and (B.13) becomes

$$Q(t) \approx 8\pi\, r_o k T_s' e^{-\frac{1}{a}\left(\frac{\pi}{r_o}\right)^2 t} \tag{B.15}$$

In fig. B.1 is given a plot of equation B.13, B.14 and B.15.

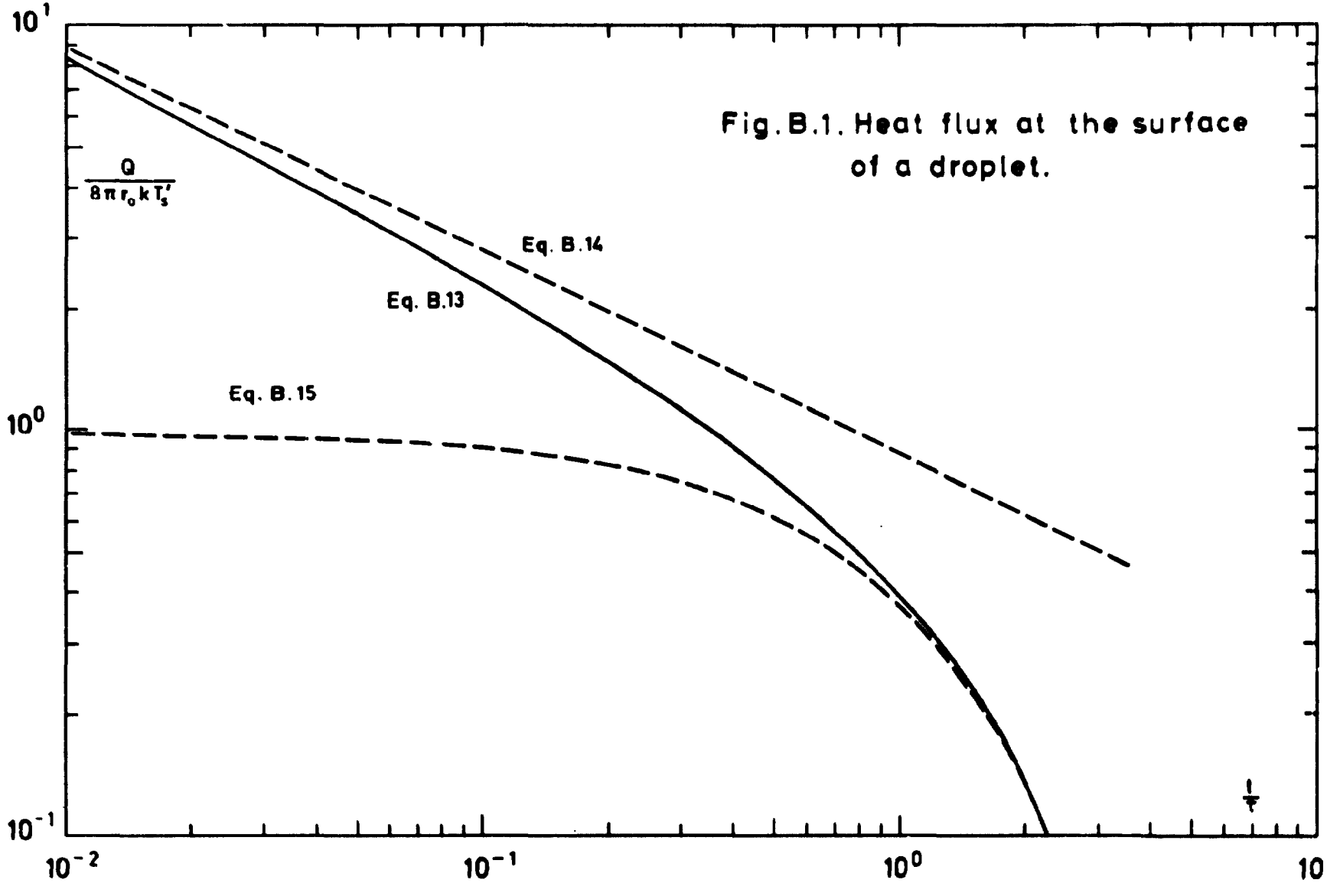

Fig. B.1. Heat flux at the surface of a droplet.

From (B.15) it is seen that the droplet for large t will have a time constant of

$$\tau = a \left(\frac{r_o}{\pi}\right)^2 \qquad \text{(B.16)}$$

For a droplet radius of 10^{-3} m $\tau \approx 0.6$ seconds.

Under the assumption that the droplet has a time constant given by (B.16), the heat transfer to the surface can be expressed by a constant factor h, and (B.1) reduces to

$$\frac{4}{3} \pi r_o^3 \rho c \frac{\partial T_m}{\partial t} = 4\pi r_o^2 h T_m \qquad \text{(B.17)}$$

where T_m is the difference between the surface temperature and the mean temperature of the droplet. It should be noted that $T_m \neq T_s'$.

Combining (B.16) and (B.17) we obtain

$$h = \frac{k}{3} \frac{\pi^2}{r_o} . \qquad \text{(B.18)}$$

APPENDIX C

Two Flux Model for a Slab Containing a Two Component Mixture

Let us consider an infinite long slab as shown in Figure C.1, and make the following assumptions.

1. Only radiation perpendicular to the slab will be considered.
2. Scattering in the two media is neglected.
3. The components ℓ and g of the medium have uniform temperatures T_ℓ and T_g, and are uniformly distributed.

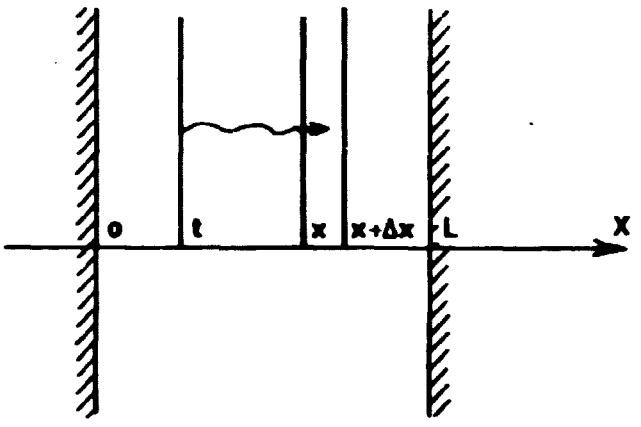

Fig. C.1. Two Flux Model for an Infinite Long Slab.

Let the flux in the positive direction be $I^+(x)$ and in the negative direction $I^-(x)$, and let a_ℓ and a_g be the absorption coefficient for the two components of the media.

The absorption in the two components in a small slab Δx will then be

$$\Delta I_\ell = -a_\ell(T_\ell)(I^+(x) + I^-(x))\Delta x \qquad (C.1)$$

$$\Delta I_g = -a_g(T_g)(I^+(x) + I^-(x))\Delta x \qquad (C.2)$$

and the total absorption will be

$$\Delta I = -(a_\ell + a_g)(I^+(x) + I^-(x))\Delta x \qquad (C.3)$$

The emission from the two components in either direction in the small slab will be

$$2B_\ell(T_\ell)\Delta x \quad \text{and} \quad 2B_g(T_g)\Delta x$$

and the total emission will be

$$2B\,\Delta x = 2(B_\ell + B_g)\Delta x \qquad (C.4)$$

Due to the symmetry around the mid-plane of the slab we have

$$I^-(x) = I^+(L-x) \qquad (C.5)$$

We are now able to make an integro-differential equation for $I^+(x)$

$$I^+(x) = B_w\, e^{-(a_\ell+a_g)x} + \int_0^x (B_\ell(T_\ell)+B_g(T_g))e^{-(a_\ell+a_g)(x-t)}dt \qquad (C.6)$$

This equation can be integrated to give

$$I^+(x) = B_w\, e^{-(a_\ell+a_g)x} + (B_\ell(T_\ell)+B_g(T_g))\,\frac{1-e^{-(a_\ell+a_g)x}}{a_\ell+a_g} \qquad (C.7)$$

Let us consider the case of thermodynamic equilibrium, i.e. $T_\ell = T_g = T_w$.

In that case there is no net energy exchange and we have that absorption equals emission, and as this is true for both components we get

$$2\,B_\ell(T_\ell) = a_\ell(T_\ell)(I^+(x)+I^-(x)) \qquad (C.8)$$

$$2\,B_g(T_g) = a_g(T_g)(I^+(x)+I^-(x)) \qquad (C.9)$$

from which we get

$$I^+(x) + I^-(x) = \text{const.} \qquad (C.10)$$

On the other hand as there is no net energy transfer across any plane in the slab we have

$$I^+(x) - I^-(x) = 0 \tag{C.11}$$

And combining (C.6), (C.10) and (C.11) we get

$$I^+(x) = I^-(x) = B_w \tag{C.12}$$

At the wall again we have no net transfer, i.e.

$$0 = \frac{\varepsilon}{1-\varepsilon} (\sigma T_w^4 - B_w) \tag{C.13}$$

and we get

$$I^+(x) = I^-(x) = \sigma T_w^4$$

Combining this with (C.8) and (C.9) and using that $T_\ell = T_g = T_w$ for thermodynamic equilibrium we get

$$B_\ell(T_\ell) = a_\ell(T_\ell)\sigma T_\ell^4 \tag{C.14}$$

$$B_g(T_g) = a_g(T_g)\sigma T_g^4 \tag{C.15}$$

Having found an expression for B_ℓ and B_g we are now able to solve the general case where $T_\ell \neq T_g \neq T_w$ and inserting (C.14) and (C.15) in (C.7) we get

$$I^+(x) = B_w e^{-(a_\ell+a_g)x} + \frac{a_\ell\sigma T_\ell^4+a_g\sigma T_g^4}{a_\ell+a_g} (1-e^{-(a_\ell+a_g)x}) \tag{C.16}$$

The incident radiation to the wall is

$$I^-(o) = I^+(L) \tag{C.17}$$

and using that

$$B_w = \varepsilon_w \sigma T_w^4 + (1 - \varepsilon_w) I^-(o) \tag{C.18}$$

we get

$$B_w = \varepsilon_w\sigma T_w^4+(1-\varepsilon_w)\left\{B_w e^{-(a_\ell+a_g)L} + \frac{a_\ell\sigma T_\ell^4+a_g\sigma T_g^4}{a_\ell+a_g} (1-e^{-(a_\ell+a_g)L})\right\} \tag{C.19}$$

Defining

$$\tau = e^{-(a_\ell+a_g)L} \tag{C.20}$$

$$\epsilon_\ell = (1-\tau)\frac{a_\ell}{a_\ell+a_g} \tag{C.21}$$

$$\epsilon_g = (1-\tau)\frac{a_g}{a_\ell+a_g} \tag{C.22}$$

$$S_w = \sigma T_w^4 \tag{C.23}$$

$$S_\ell = \sigma T_\ell^4 \tag{C.24}$$

$$S_g = \sigma T_g^4 \tag{C.25}$$

we get

$$B_w = \epsilon_w S_w + (1-\epsilon_w)\{B_w\tau + \epsilon_\ell S_\ell + \epsilon_g S_g\} \tag{C.26}$$

which can be rewritten to

$$\frac{\epsilon_w}{1-\epsilon_w}(S_w-B_w) + \epsilon_\ell(S_\ell-B_w) + \epsilon_g(S_g-B_w) = 0 \tag{C.27}$$

The net heat transfer to the ℓ component per area unit of the wall is

$$Q_e = \int_0^L I^+(x)\, a_\ell\, dx - \int_0^L a_\ell\, \sigma\, T_\ell^4\, dx$$

$$= (B_w-S_\ell)\epsilon_\ell + (S_g-S_\ell)\frac{a_\ell a_g L}{a_\ell+a_g}\left\{1 - \frac{1-\tau}{(a_\ell+a_g)L}\right\} \tag{C.28}$$

And similar for the net heat transfer to the g component we get

$$Q_g = (B_w-S_g)\epsilon_g + (S_\ell-S_g)\frac{a_\ell a_g L}{a_\ell+a_g}\left\{1 - \frac{1-\tau}{(a_\ell+a_g)L}\right\} \tag{C.29}$$

Defining

$$R_{\ell g} = \left\{\frac{a_\ell a_g L}{a_\ell+a_g}\left(1 - \frac{1-\tau}{(a_\ell+a_g)L}\right)\right\}^{-1} \tag{C.30}$$

we obtain an electrical analog as shown in Figure C.2.

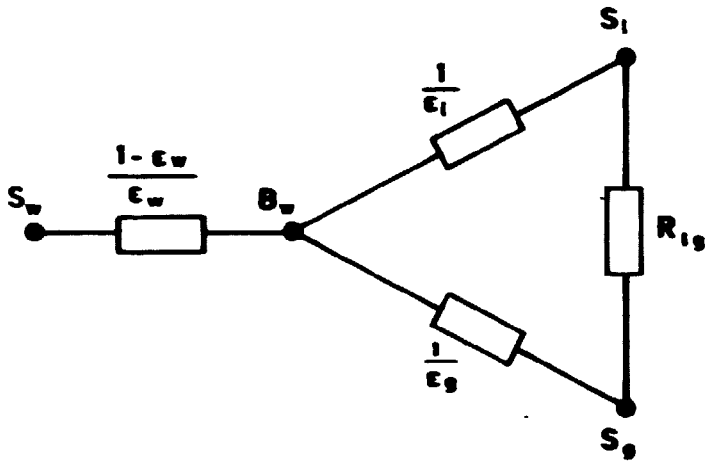

Fig.C.2. Electrical Analog.

It should be noted that the assumption of a uniform temperature of the two media can generally only be made in the optically thin limit. In this case R_{lg} reduces to

$$R_l^{-1} = \tfrac{1}{2}(a_l L)(a_g L) + o(L^2) \qquad (C.31)$$

Accordingly if the optical thin assumption, which is a first order approximation, is made, the direct interchange between the two components as a second order term can be neglected.

ISBN 87-550-0565-9
ISSN 0418-6435